Supplementary Information for "Nonreciprocal quantum synchronization"

Deng-Gao Lai,[1,*] Adam Miranowicz,[1,2] and Franco Nori[1,3]

[1]*RIKEN Center for Quantum Computing (RQC), 2-1 Hirosawa, RIKEN Wako-shi, Saitama 351-0198, Japan*
[2]*Institute of Spintronics and Quantum Information, Faculty of Physics and Astronomy, Adam Mickiewicz University, 61-614 Poznań, Poland*
[3]*Physics Department, University of Michigan, Ann Arbor, Michigan 48109-1040, USA*

In this Supplementary Material, we provide comprehensive insights into the nonreciprocal quantum synchronization of phonons, highlighting its counterintuitive robustness against both imperfections and thermal noise of practical devices. This document comprises the following contents on important aspects of our investigation: originality, novelty, and significance of our work; system parameters; quantum Langevin equations and quantum synchronization measure; quantum nonreciprocity enabled by the synergy of the Sagnac and magnon-Kerr effects; nonreciprocal quantum synchronization; context of the synchronization theory; and potential applications of our study.

Contents

*Electronic address: denggaolai@foxmail.com

I. SUPPLEMENTARY NOTES

A. Originality, novelty, and significance of our work

In this section, we highlight the originality, novelty, and significance of our work, and demonstrate the broad applicability and universality of our approach.

(i) Nonreciprocal quantum synchronization of phonon modes remains unexplored.—Nonreciprocal physics is garnering enormous attention in both classical and quantum research fields. Surprisingly, previous demonstrations have not explored nonreciprocal quantum synchronization of phonons, one of the most obvious examples of nonreciprocal quantum resources. Here we fill this gap to demonstrate the possibility of nonreciprocal quantum synchronization, revealing its counterintuitive robustness against random fabrication imperfections and thermal noise of practical devices. The study lays the foundation for generating fragile-to-robust nonreciprocal quantum resources. To our knowledge, we are the first to study nonreciprocal quantum synchronization via the synergy of the Sagnac and magnon-Kerr effects. While the use of the Sagnac effect to achieve the nonreciprocity of the optical transmission [S1] and photon blockade [S2] has been studied, its application to quantum synchronization has not been explored to date. Inspired by the Sagnac-effect-induced nonreciprocity mechanism [S1], we introduce a fundamentally different nonreciprocity mechanism based on the magnon-Kerr effect and demonstrate the first realization of nonreciprocal quantum synchronization, revealing its counterintuitive robustness against both random fabrication imperfections and thermal noise of practical devices.

(ii) Our idea is not a simple synergy of the Sagnac and magnon-Kerr effects, but rather the generation of novel nonreciprocal quantum phenomena and addressing an outstanding challenge, i.e., quantum synchronization is extremely sensitive to random fabrication imperfections and thermal noise of practical devices.—Specifically, quantum synchronization of phonon modes is generally deteriorated or even completely destroyed by thermal noise and random fabrication imperfections. Surprisingly, our proposal overcomes this obstacle and generates a unique one-way quantum synchronization robust to these detrimental factors, without the need of using any high-cost, low-loss materials or noise filters at the expense of the system complexity.

(iii) Significance to the field.—(1) We believe our work offers both conceptual and technical advances that are broadly relevant to the field of cavity opto-magnon-mechanics. The demonstrated ability to achieve nonreciprocal quantum synchronization via both the Sagnac effect and magnon-Kerr nonlinearity opens a new pathway for an active control of one-way nonequilibrium quantum dynamics in hybrid quantum platforms. These results are expected to be of interest also to researchers in quantum phononics, nonlinear quantum dynamics, and quantum information, where robust and tunable quantum synchronization and its quantum nonreciprocity are highly desirable. (2) Our work presents an innovative approach to reversing the intrinsically detrimental effects of practical devices, and paves a general route to pioneering nonreciprocal quantum resources, with robustness against both random fabrication imperfections and thermal noise of practical devices. (3) Our study exhibits broad applicability and universality. Beyond nonreciprocal quantum synchronization, our approach applies broadly to one-way quantum phenomena, including nonreciprocal entanglement and nonreciprocal topological phonon transfer.

(iv) Comparison with Existing Literatures.—Prior studies have investigated quantum synchronization in optomechanical systems [S3] nonreciprocal transport of information or photons using the Sagnac effect [S1, S2], and magnon-Kerr nonlinearity in YIG-based systems [S4]. However, our work brings together these ingredients in a previously unexplored regime: (1) The sign and strength of the magnon-Kerr nonlinearity are tuned in situ via the external magnetic field, allowing dynamical control over the coupling landscape. (2) Nonreciprocal quantum synchronization is modulated by optical driving directions or external magnetic field directions, enabled by the Sagnac effect in a spinning microsphere or the magnon-Kerr effect in a YIG sphere, respectively. (3) Quantum synchronization becomes effectively nonreciprocal, without requiring additional gain or engineered reservoirs. To our knowledge, no previous study has demonstrated this level of nonreciprocal control over quantum synchronization and unidirectional phononic coupling via combined photonic, phononic, and magnonic pathways. We are neither aware of any prior established demonstration that reports this combination of these mechanisms, nor one that realizes tunable nonreciprocal quantum synchronization in this manner.

(v) In a broader view, our study presents an innovative approach to reversing the intrinsically detrimental effects of practical devices.—It paves a general route to pioneering nonreciprocal quantum resources, with robustness against both random fabrication imperfections and thermal noise of practical devices.

(vi) Our approach has a broad applicability and universality.—Our framework is not limited to a specific unidirectional quantum effect such as nonreciprocal quantum synchronization, but extends to a broader class of one-way quantum phenomena, including nonreciprocal quantum entanglement and unidirectional topological phonon transfer. For example: (1) our framework naturally extends to nonreciprocal quantum entanglement between two phonon modes, and (2) it can be generalized to explore nonreciprocal topological phononics and photonics, as described in Fig. 3(g) of the main text.

Symbols	Physical quantities	Simulation parameters [S2, S3, S6]	Experimental parameters [S1, S4, S5, S7]
c	Vacuum light speed	3×10^8 m/s	3×10^8 m/s
λ	Laser wavelength	1550 nm	1550 nm
γ	Gyromagnetic ratio	$2\pi \times 2.8$ MHz/Oe	$2\pi \times 2.8$ MHz/Oe
H	Bias magnetic field of the YIG sphere	Above its saturation magnetization ($H > 1750$ Oe)	Above its saturation magnetization ($H > 1750$ Oe)
$\omega_1/2\pi$	Resonance frequency of the first resonator	10 MHz	15.25 MHz
$\omega_2/2\pi$	Resonance frequency the second resonator	10.05 MHz	15.367 MHz
Δ_a/ω_1	Optical detuning	-1.005	± 1.008
Δ_m/ω_1	Magnonic detuning	-1	± 1
K/ω_1	Magnon-Kerr coefficient	-5×10^{-5} to 5×10^{-5}	0
κ_a/ω_1	Optical decay rate	0.15	0.66
κ_m/ω_1	Magnon decay rate	0.2	0.066
γ_j/ω_1	Mechanical damping rates	0.005	0.0003 (0.0004)
m_j, m_0	Effective masses of resonators	100 ng	100 (50) ng
$\bar{n}_j$	Bath mean phonon numbers	0 to 10^4	Not shown
N_a	Mean photon number	$N_a = \langle a^\dagger a \rangle$	$N_a = \langle a^\dagger a \rangle$
N_m	Mean magnon number	$N_m = \langle m^\dagger m \rangle$	$N_m = \langle m^\dagger m \rangle$
$G_a/\omega_1 = g_a\sqrt{N_a}/\omega_1$	Effective photon-phonon coupling strength	$0 \sim 0.2$	$0 \sim 0.1$
$G_m/\omega_1 = g_m\sqrt{N_m}/\omega_1$	Effective magnon-phonon coupling strength	$0 \sim 0.2$	$0 \sim 0.1$
χ/ω_1	Phonon-phonon coupling rate	0.02	0.0003
$\xi_{a(m)}/\omega_1$	Driving intensity	35	Not shown
Ω	Spinning angular velocity	0 to 10 kHz	0
$\varepsilon_{0(j=1,2)}$	Dielectric constants of air (taper, silica sphere)	1 (3.9)	1 (3.9)
ζ	Refractive indexes of silica sphere	1.486	1.486
r	Silica microsphere radii	1.1 mm	0.2 mm
r_0	YIG microsphere radii	0.5 mm	0.2 mm
E	Young modulus of silica	75 GPa	75 GPa
Υ	Elastic limit of silica	9 GPa	9 GPa

TABLE I: Parameters of the hybrid quantum devices set in our simulations [S2, S3, S6] and in reported experiments [S1, S4, S5, S7]. Columns 1 and 2 present the parameter symbols and their physical meanings, respectively. The parameters in columns 3 and 4 are used in our numerical simulations [S2, S3, S6] and the state-of-the-art experiments [S1, S4, S5, S7], respectively. The close agreement between experimentally reported parameters and those used in our simulations demonstrates the experimental feasibility of the proposed phenomena, highlighting their relevance to current state-of-the-art platforms.

B. System parameters

A comprehensive overview of the symbols and system parameters employed in this study is provided in Tab. I. All system parameters used in our numerical simulations have been explicitly provided, closely consistent with those values reported in previous studies [S1–S7]. Note that we set $\omega_1 = 2\pi \times 10$ MHz as a reference unit of frequency, and all physical parameters used in the simulations are listed. Although what we have proposed a purely theoretical scheme, our approach is completely experimentally feasible, using the state-of-the-art experimental conditions (see Tab. I). It demonstrates the consistency between the parameters used in our numerical simulations [S2, S3, S6] and those reported in realistic experiments [S1, S4, S5, S7], indicating that the proposed phenomena are experimentally accessible with current state-of-the-art platforms. Moreover, all claims made in the manuscript are directly supported by our analytical derivations and numerical simulations based on a set of coupled quantum Langevin equations, which capture the essential physics of the hybrid photon-phonon-magnon system. Each of

the central results arises naturally from the hybrid quantum opto-magnon-mechanical model and has been systematically tested across a broad and experimentally realistic (state-of-the-art) parameter spaces, as shown in Tab. I. Our results reveal that the effectiveness of the scheme extends well beyond the previous parameter choices [S3], demonstrating robust performance over a wide range of parameter space. The system parameters, boundary conditions, and dynamical regimes are clearly stated, and the outcomes are consistent with the underlying physical mechanisms.

Note that in fact, the values of the quantum synchronization parameters are not constrained to strictly follow those in Ref. [S3], but remain highly effective over a wide range of parameter settings. To demonstrate this, we have plotted the quantum synchronization measure versus each system parameters when the magnon-Kerr strength is absence and presence. Our results reveal that the effectiveness of the scheme extends well beyond the parameter choices in Ref. [S3], demonstrating robust performance across a broad range of parameter regimes.

II. SUPPLEMENTARY METHODS

A. Quantum Langevin equations and quantum synchronization measure

In this section, we derive the quantum Langevin equations of a hybrid quantum system, which consists of a silica microsphere coupled to a YIG microsphere. We find their solutions, demonstrate the magnon-Kerr-nonlinearity-induced transition between the redshift and blueshift, and show the measure of quantum synchronization.

1. Physical model and its Hamiltonian

We focus on a hybrid quantum platform consisting of a silica microsphere (i.e., optomechanical cavity) in combination with a YIG microsphere (i.e., magnomechanical cavity), coherently coupled to each other via a direct physical contact. Note that the described system has already been implemented with state-of-the-art technology to enable new architectures for coherent coupling between magnons, phonons, and photons [S5]. The vibration of the silica (YIG) microsphere is explored by the radiation-pressure (magnetostrictive) force through the circulating-optical fields (microwave-driven magnons). Specifically, a uniform magnon mode is supported by a YIG microsphere using an external magnetic field H, and the magnetostrictive force, exciting phonons in the YIG microsphere by a microwave, leads to the coupling of the magnon mode to the vibrational mode. In the silica microsphere, a phonon mode is coupled to an optical mode via the radiation-pressure and photoelastic effects; meanwhile, imposing the direct physical contact of the two microspheres engenders a direct coupling between two localized vibrational modes. This hybrid quantum platform is established to exploit tunable interactions between phonons, photons, and magnons, enabling a wide range of promising applications, such as none-way quantum mechanical effects of opto- and magno-phonon motions. Then, the Hamiltonian of the physical system reads (with $\hbar = 1$):

$$\begin{aligned}\mathcal{H} &= \sum_{o=a,m}\omega_o o^\dagger o + \sum_{j=1,2}\omega_j b_j^\dagger b_j - g_m m^\dagger m(b_1^\dagger + b_1) - g_a a^\dagger a(b_2^\dagger + b_2) - \chi(b_1^\dagger b_2 + b_2^\dagger b_1)\\ &\quad + \mathrm{K}(m^\dagger m)^2 + i\left(\xi_a a^\dagger e^{-i\omega_{d,a}t} - \xi_a^* a e^{i\omega_{d,a}t}\right) + i\left(\xi_m m^\dagger e^{-i\omega_{d,m}t} - \xi_m^* m e^{i\omega_{d,m}t}\right),\end{aligned} \tag{S1}$$

where $a^\dagger$ (a), $m^\dagger$ (m), and $b_j^\dagger$ (b_j) denote the creation (annihilation) operators of the photon, magnon, and phonon modes supported in silica and YIG microspheres, with the resonance frequencies of ω_a, ω_m, and ω_j, respectively. The g_a and g_m terms are, respectively, the photon- and magnon-phonon interactions. The phonon-phonon coupling with strength χ arises from direct physical contact between a spinning silica microsphere and a counter-spinning YIG sphere, with both maintaining a constant rotational angular velocity Ω throughout the process. The K term describes the magnon-Kerr nonlinearity [S4], which is introduced to generate nonreciprocity. The term ξ_m is the driving field of the microwave with frequency $\omega_{d,m}$, and the term ξ_a is the driving field of the optical mode a with frequency $\omega_{d,a}$.

2. Quantum Langevin equations and their solutions

In a realistic experiment [S5], the proposed hybrid quantum platform comprises a YIG sphere (serving as a magnomechanical cavity) and a silica microsphere (serving as an optomechanical cavity), both of which are coherently coupled to each other via direct physical contact. In the silica microsphere, the phonon mode is driven by the radiation-pressure interaction from circulating optical fields; whereas in the YIG sphere, it is excited via magnetostrictive forces mediated by microwave-driven magnons. Specifically, a uniform magnon mode, supported by the YIG sphere under an external magnetic field, couples to a phonon mode via magnetostrictive interaction [S7, S8], enabling microwave excitation of phonons in the YIG sphere. In the silica

microsphere supporting a radiation-pressure-induced mechanical radial breathing mode, the optical mode and the mechanical radial mode are intrinsically coupled through radiation pressure and the photoelastic effect [S9–S11], forming a canonical optomechanical interaction. Meanwhile, the direct physical contact between the silica and YIG microspheres establishes an effective mechanical coupling of their localized phonon modes. In the YIG sphere, microwave driving of the magnon mode excites the phonon mode via the magnomechanical effect [S12]. Bringing the silica microsphere into direct contact with the YIG sphere establishes a mechanical coupling between their spatially separated phonon modes. Simultaneously, radiation-pressure-induced optomechanical coupling in the silica cavity plays a key role in the hybrid quantum dynamics. The process involves a synergistic interplay of optomechanics, magnomechanics, phonon interference, and quantum mechanical effects [S13, S14], wherein microwave and optical signals are coherently mapped onto two nearly degenerate mechanical modes, enabling their interference [S15, S16].

In a rotating frame, defined by the unitary transformation operator $\exp[-i(\omega_{d,a}a^\dagger a+\omega_{d,m}m^\dagger m)t]$, the Hamiltonian of the hybrid system becomes

$$\begin{aligned}\mathcal{H}_I &= \Delta_a a^\dagger a + \Delta_m m^\dagger m + \omega_1 b_1^\dagger b_1 + \omega_2 b_2^\dagger b_2 - g_m m^\dagger m(b_1^\dagger + b_1) - g_a a^\dagger a(b_2^\dagger + b_2) - \chi(b_1^\dagger b_2 + b_2^\dagger b_1) \\ &\quad + \mathrm{K}(m^\dagger m)^2 + i(\xi_a a^\dagger - \xi_a^* a) + i(\xi_m m^\dagger - \xi_m^* m),\end{aligned} \tag{S2}$$

where the parameter $\Delta_{o=a,m} = \omega_o - \omega_{d,o}$ is the driving detuning between the cavity mode frequency ω_a or the magnetic mode frequency ω_m and the corresponding driving frequency $\omega_{d,o}$ for $o = a, m$.

By phenologically adding the dissipation and noise terms into the Heisenberg equations, the quantum Langevin equations of this hybrid system can be obtained as:

$$\dot{a} = -i\Delta_a a + ig_a a(b_2 + b_2^\dagger) - \kappa_a a + \xi_a + \sqrt{2\kappa_a}a_{\mathrm{in}}, \tag{S3a}$$

$$\dot{m} = -i\Delta_m m - i2\mathrm{K}m^\dagger mm + ig_m m(b_1 + b_1^\dagger) - \kappa_m m + \xi_m + \sqrt{2\kappa_m}m_{in}, \tag{S3b}$$

$$\dot{b}_1 = -i\omega_1 b_1 + ig_m m^\dagger m + i\chi b_2 - \gamma_1 b_1 + \sqrt{2\gamma_1}b_{1,\mathrm{in}}, \tag{S3c}$$

$$\dot{b}_2 = -i\omega_2 b_2 + ig_a a^\dagger a + i\chi b_1 - \gamma_2 b_2 + \sqrt{2\gamma_2}b_{2,\mathrm{in}}, \tag{S3d}$$

where $\kappa_{o=a,m}$ and $\gamma_{j=1,2}$ are the decay rates of the optical/magnon mode and the jth phonon modes, respectively. In addition, the operators o_{in} and $b_{j,\mathrm{in}}$ are, respectively, the zero-mean input noise operators for the optical/magnon mode and the jth motional mode, characterized by the following correlation functions:

$$\langle a_{\mathrm{in}}a_{\mathrm{in}}^\dagger\rangle = \delta(t-t'), \ \ \langle a_{\mathrm{in}}^\dagger a_{\mathrm{in}}\rangle = 0, \tag{S4a}$$

$$\langle m_{\mathrm{in}}m_{\mathrm{in}}^\dagger\rangle = \delta(t-t'), \ \ \langle m_{\mathrm{in}}^\dagger m_{\mathrm{in}}\rangle = 0, \tag{S4b}$$

$$\langle b_{1,\mathrm{in}}b_{1,\mathrm{in}}^\dagger\rangle = (\bar{n}_1+1)\delta(t-t'), \ \ \langle b_{1,\mathrm{in}}^\dagger b_{1,\mathrm{in}}\rangle = \bar{n}_1\delta(t-t'), \tag{S4c}$$

$$\langle b_{2,\mathrm{in}}b_{2,\mathrm{in}}^\dagger\rangle = (\bar{n}_2+1)\delta(t-t'), \ \ \langle b_{2,\mathrm{in}}^\dagger b_{2,\mathrm{in}}\rangle = \bar{n}_2\delta(t-t'), \tag{S4d}$$

where the parameter $\bar{n}_{j=1,2} = \left\{\exp[\hbar\omega_j/(k_B T_j)] - 1\right\}^{-1}$ denotes the average thermal phonon numbers associated with the heat bath of the jth vibrational mode, with k_B being the Boltzmann constant and T_j being the bath temperature of the jth motional mode. By considering the strong-driving regime of the hybrid quantum system, we can easily simplify the proposed physical model. Specifically, we express the operators in Eqs. (S8) as sums of their classical means and quantum fluctuations, i.e.,

$$a = \langle a\rangle + \delta a, \ \ a^\dagger = \langle a^\dagger\rangle + \delta a^\dagger, \tag{S5a}$$

$$m = \langle m\rangle + \delta m, \ \ m^\dagger = \langle m^\dagger\rangle + \delta m^\dagger, \tag{S5b}$$

$$b_j = \langle b_j\rangle + \delta b_j, \ \ b_j^\dagger = \langle b_j^\dagger\rangle + \delta b_j^\dagger. \tag{S5c}$$

In the following we denote:

$$\langle a\rangle = \alpha, \ \ \langle a^\dagger\rangle = \alpha^*, \tag{S6a}$$

$$\langle m\rangle = \mu, \ \ \langle m^\dagger\rangle = \mu^*, \tag{S6b}$$

$$\langle b_j\rangle = \beta_j, \ \ \langle b_j^\dagger\rangle = \beta_j^*. \tag{S6c}$$

By separating the classical motion and quantum fluctuations, the equations of motion for the classical-motion variables can be obtained as:

$$\dot{\alpha} = -i\Delta_a\alpha + ig_a\alpha(\beta_2^* + \beta_2) - \kappa_a\alpha + \xi_a, \tag{S7a}$$

$$\dot{\mu} = -i\Delta_m\mu - i2\mathrm{K}\mu^*\mu\mu + ig_m\mu(\beta_1^* + \beta_1) - \kappa_m\mu + \xi_m, \tag{S7b}$$

$$\dot{\beta}_1 = -i\omega_1\beta_1 + ig_m\mu^*\mu + i\chi\beta_2 - \gamma_1\beta_1, \tag{S7c}$$

$$\dot{\beta}_2 = -i\omega_2\beta_2 + ig_a\alpha^*\alpha + i\chi\beta_1 - \gamma_2\beta_2, \tag{S7d}$$

where $2\mathrm{K}\mu^*\mu$ is the shift of the detuning, resulted from the self-Kerr effect of the magnon mode. After safely separating the classical motions, the Langevin equations of motion for quantum fluctuations can be rewritten as:

$$\delta\dot{a} = -i\Delta_a'\delta a + ig_a\alpha(\delta b_2 + \delta b_2^\dagger) - \kappa_a\delta a + \sqrt{2\kappa_a}a_{\mathrm{in}}, \tag{S8a}$$

$$\delta\dot{m} = -i\Delta_m'\delta m - i2\mathrm{K}\mu\mu\delta m^\dagger + ig_m\mu(\delta b_1 + \delta b_1^\dagger) - \kappa_m\delta m + \sqrt{2\kappa_m}m_{\mathrm{in}}, \tag{S8b}$$

$$\delta\dot{b}_1 = -i\omega_1\delta b_1 + ig_m\mu^*\delta m + ig_m\mu\delta m^\dagger + i\chi\delta b_2 - \gamma_1\delta b_1 + \sqrt{2\gamma_1}b_{1,\mathrm{in}}, \tag{S8c}$$

$$\delta\dot{b}_2 = -i\omega_2\delta b_2 + ig_c\alpha^*\delta a + ig_c\alpha\delta a^\dagger + i\chi\delta b_1 - \gamma_2\delta b_2 + \sqrt{2\gamma_2}b_{2,\mathrm{in}}, \tag{S8d}$$

where

$$\Delta_a' = \Delta_a - g_a(\beta_2^* + \beta_2) = \Delta_a - 2g_a\mathrm{Re}[\beta_2], \tag{S9a}$$

$$\Delta_m' = \Delta_m - g_m(\beta_1^* + \beta_1) + 4\mathrm{K}\mu^*\mu = \Delta_m - 2g_m\mathrm{Re}[\beta_1] + 4\mathrm{K}\mu^*\mu, \tag{S9b}$$

are the normalized detunings of the cavity-field and magnon modes, respectively. In the above equations, we can rewrite μ and α as $\mu = \mathrm{Re}[\mu] + i\mathrm{Im}[\mu]$ and $\alpha = \mathrm{Re}[\alpha] + i\mathrm{Im}[\alpha]$, respectively. By defining the photon, magnon, and phonon quadratures and the corresponding Hermitian input noise operators as:

$$X_o = (\delta o^\dagger + \delta o)/\sqrt{2}, \qquad Y_o = i(\delta o^\dagger - \delta o)/\sqrt{2}, \tag{S10a}$$

$$X_o^{\mathrm{in}} = (\delta o_{\mathrm{in}}^\dagger + \delta o_{\mathrm{in}})/\sqrt{2}, \quad Y_o^{\mathrm{in}} = i(\delta o_{\mathrm{in}}^\dagger - \delta o_{\mathrm{in}})/\sqrt{2}, \tag{S10b}$$

for the operators $o = a,\ m,\ b_1,\ b_2$. The Langevin equations of motion for quantum fluctuations can be reexpressed as a compact form:

$$\dot{\mathbf{u}}(t) = \mathbf{A}\mathbf{u}(t) + \mathbf{N}(t), \tag{S11}$$

where we introduce the fluctuation operator vector

$$\mathbf{u}(t) = [X_a, Y_a, X_m, Y_m, X_{b_1}, Y_{b_1}, X_{b_2}, Y_{b_2}]^T, \tag{S12}$$

the noise operator vector

$$\mathbf{N}(t) = \sqrt{2}[\sqrt{\kappa_a}X_a^{\mathrm{in}},\ \sqrt{\kappa_a}Y_a^{\mathrm{in}},\ \sqrt{\kappa_m}X_m^{\mathrm{in}},\ \sqrt{\kappa_m}Y_m^{\mathrm{in}},\ \sqrt{\gamma_1}X_{b_1}^{\mathrm{in}},\ \sqrt{\gamma_1}Y_{b_1}^{\mathrm{in}},\ \sqrt{\gamma_2}X_{b_2}^{\mathrm{in}},\ \sqrt{\gamma_2}Y_{b_2}^{\mathrm{in}}]^T, \tag{S13}$$

and the coefficient matrix

$$\mathbf{A} = \begin{bmatrix} -\kappa_a & \Delta_a' & 0 & 0 & 0 & 0 & -2g_a\mathrm{Im}[\alpha] & 0 \\ -\Delta_a' & -\kappa_a & 0 & 0 & 0 & 0 & 2g_a\mathrm{Re}[\alpha] & 0 \\ 0 & 0 & -(\kappa_m - 4\mathrm{KRe}[\mu]\mathrm{Im}[\mu]) & \Delta_m' - 2\mathrm{K}(\mathrm{Re}[\mu]^2 - \mathrm{Im}[\mu]^2) & -2g_m\mathrm{Im}[\mu] & 0 & 0 & 0 \\ 0 & 0 & -(\Delta_m' + 2\mathrm{K}(\mathrm{Re}[\mu]^2 - \mathrm{Im}[\mu]^2)) & -(\kappa_m + 4\mathrm{KRe}[\mu]\mathrm{Im}[\mu]) & 2g_m\mathrm{Re}[\mu] & 0 & 0 & 0 \\ 0 & 0 & 0 & 0 & -\gamma_1 & \omega_1 & 0 & -\chi \\ 0 & 0 & 2g_m\mathrm{Re}[\mu] & 2g_m\mathrm{Im}[\mu] & -\omega_1 & -\gamma_1 & \chi & 0 \\ 0 & 0 & 0 & 0 & 0 & -\chi & -\gamma_2 & \omega_2 \\ 2g_a\mathrm{Re}[\alpha] & 2g_a\mathrm{Im}[\alpha] & 0 & 0 & \chi & 0 & -\omega_2 & -\gamma_2 \end{bmatrix}. \tag{S14}$$

A formal solution of the Langevin equation (S11) is given by

$$\mathbf{u}(t) = \mathbf{M}(t)\mathbf{u}(0) + \int_0^t \mathbf{M}(t-s)\mathbf{N}(s)ds, \tag{S15}$$

where $\mathbf{M}(t) = \exp(\mathbf{A}t)$. Note that the parameters chosen for all our numerical simulations satisfy the stability conditions derived from the Routh-Hurwitz criterion. Namely, the real parts of all the eigenvalues of $\mathbf{A}$ are negative.

For studying the quantum synchronization between the opto- and magnon-mechanical vibrations, we calculate the covariance matrix $\mathbf{V}$, which is defined by the matrix elements

$$\mathbf{V}_{k,l}(t) = \frac{1}{2}[\langle \mathbf{u}_k(t)\mathbf{u}_l(t)\rangle + \langle \mathbf{u}_l(t)\mathbf{u}_k(t)\rangle], \tag{S16}$$

for k, l = 1-8. Under the stability condition, the covariance matrix $\mathbf{V}(t)$ fulfills the Lyapunov equation,

$$\dot{\mathbf{V}}(t) = \mathbf{A}\mathbf{V} + \mathbf{V}\mathbf{A}^T + \mathbf{Q}, \tag{S17}$$

where we introduce the matrix

$$\mathbf{Q} = \frac{1}{2}(\mathbf{C} + \mathbf{C}^T), \tag{S18}$$

with $\mathbf{C}$ being the noise correlation matrix, which can be defined through the matrix elements,

$$\langle \mathbf{N}_k(s)\mathbf{N}_l(s')\rangle = \mathbf{C}_{k,l}\delta(s - s'). \tag{S19}$$

In terms of Eqs. (S13), (S18), and (S19), the expression of the matrix $\mathbf{Q}$ can be obtained as

$$\mathbf{Q} = \mathrm{diag}\{\kappa_a, \kappa_a, (2\bar{n}_m + 1)\kappa_m, (2\bar{n}_m + 1)\kappa_m, (2\bar{n}_1 + 1)\gamma_1, (2\bar{n}_1 + 1)\gamma_1, (2\bar{n}_2 + 1)\gamma_2, (2\bar{n}_2 + 1)\gamma_2\}. \tag{S20}$$

Based on Eqs. (S14), (S16), (S17), and (S20), we can obtain the covariance matrix $\mathbf{V}$. Then, the quantum synchronization of the opto- and magnon-mechanical vibrations can be achieved.

3. *Quantum synchronization measure*

In purely classical contexts, synchronization is primarily explored within autonomous nonlinear systems experiencing limit cycles or chaotic dynamics. Complete synchronization occurs when two subsystems initially in independent configurations attain identical trajectories due to mutual interactions. For two continuous-variable (CV) classical systems described by dimensionless canonical variables $O_{b_j}(t)$ ($O \in \{X, Y\}$) representing the evolution of two subsystems in phase space, a complete synchronization is attained when the quantities

$$O_-(t) := \left[O_{b_1}(t) - O_{b_2}(t)\right] / \sqrt{2} \tag{S21}$$

approach zero asymptotically for sufficiently large times [S3]. Extending the aforementioned concepts to *quantum* mechanical systems poses challenges, as fundamental limits may exist that hinder the exact fulfillment of the conditions described above. Specifically, by defining dimensionless quantities $O_{b_j}(t)$ as the quadrature operators satisfying the canonical commutation rules [S17, S18]

$$[X_{b_j}(t), Y_{b_{j'}}(t)] = i\delta_{jj'}, \tag{S22}$$

the relative coordinates $O_-(t)$ can represent the generalized position and momentum operators for the same (antisymmetric) mode. Consequently, the uncertainty principle precludes satisfying the precise condition necessary for a complete classical synchronization. To quantify this, we designate $O_-(t)$ as synchronization errors and introduce the following metric:

$$\mathcal{S}_C(t) := \Big\langle \sum_O O_-(t)^2 \Big\rangle^{-1}, \quad \text{for} \quad O = X, Y, \tag{S23}$$

quantifying the extent of complete synchronization achieved by the system, where $\langle \cdots \rangle$ denotes the expectation value taken with respect to the density matrix of quantum systems. Then, we obtain the Heisenberg principle requiring

$$\langle X_-(t)^2\rangle\langle Y_-(t)^2\rangle \geqslant 1/4, \tag{S24}$$

and therefore

$$\mathcal{S}_C(t) \leqslant \left[\langle X_-(t)^2\rangle\langle Y_-(t)^2\rangle\right]^{-1/2}/2 \leqslant 1, \tag{S25}$$

establishing a universal limit on the complete synchronization achievable between two CV systems. Conversely, in a purely classical framework, $\mathcal{S}_C(t)$ is theoretically unbounded [S3]. A small value of $\mathcal{S}_C(t)$ arises from two sources: (i) non-zero mean values of $O_-(t)$, and/or (ii) significant variances in these operators. The former scenario can be seen as a classical systematic error [S3]; whereas the latter stems from the effects of thermal and quantum noise. We can readily eliminate classical systematic errors from the synchronization measurement in Eq. (S23) just following a change of variables [S3]:

$$O_-(t) \to \delta O_-(t) = O_-(t) - \langle O_-(t)\rangle. \tag{S26}$$

This gives rise to quantum synchronization measure of phonons:

$$\mathcal{S}_Q(t) := \Big\langle \sum_O \delta O_-(t)^2 \Big\rangle^{-1}, \quad \text{for} \quad O = X, Y, \tag{S27}$$

for studying *purely* quantum mechanical effects. Note that the quantum synchronization happens when

$$\mathcal{S}_Q > 0, \tag{S28}$$

but not when

$$\mathcal{S}_Q = 0. \tag{S29}$$

Especially, an excellent quantum synchronization is implemented when

$$\mathcal{S}_Q = 1. \tag{S30}$$

Note that synchronization is classified into classical and quantum synchronization, which are, respectively, inherently robust and fragile to dephasing effects originating from thermal noise and random fabrication imperfections. Our work here is focused only on quantum synchronization but not the classical one. In our simulations, to ensure the system stability, we choose experimentally feasible parameters, as given in Tab. I.

In this work, our intention is to provide a concise and self-contained summary of the quantum synchronization parameter as introduced in Ref. [S3], which is foundational to our subsequent analysis. We focus on the coupled continuous-variable quantum systems based on cavity opto-magno-mechanics. Currently, in cavity optomechanics, the diagnostic $\mathcal{S}_Q$ [S3] is generally used to describe the measure of quantum synchronization in continuous-variable systems. While some concerns regarding the quantum synchronization measurement, it is undeniable that this method remains the most widely recognized and commonly used in cavity opto-magno-mechanical continuous-variable systems. This measurement method develops a consistent and quantitative theory of synchronization for continuous variable systems evolving in the quantum regime. Specifically, the quantum-synchronization measure $\mathcal{S}_Q$ of continuous variable systems has been introduced by extrapolating it from notions of complete synchronization that is introduced for classical models. Note that our method on the quantum-synchronization measure $\mathcal{S}_Q$ in continuous-variable systems is based on this well-known work [S3], which introduces and characterizes the measure quantifying the level of quantum synchronization of coupled continuous variable systems. This measure enables the extension of synchronization concepts into the quantum domain, and the Heisenberg principle sets a universal limitation to complete synchronization.

In particular, we here need to highlight the methodological soundness and the high standards maintained throughout this work. Our theoretical framework is based on a set of quantum Langevin equations that capture the coupled dynamics of optical, mechanical, and magnonic modes in the presence of both intrinsic dissipation and external driving. This approach is well established in the studies of cavity optomechanics and cavity optomagnonics, and has been carefully adapted here to combine the key features of our hybrid platform, including the magnon-Kerr nonlinearity, the optical Sagnac effect, and the direct phonon-phonon contact coupling. We have verified the validity of our methodology by performing extensive numerical simulations across a wide range of state-of-the-art realistic experimental parameters (see Tab. I), ensuring that our main effects are not artifacts of fine-tuning. Furthermore, the quantum synchronization dynamics are quantified using a continuous-variable measure consistent with the prior literature [S3], and the emergence of purely quantum nonreciprocity is traced analytically to the combination of the Sagnac effect and magnon-Kerr nonlinearity. We believe that the methodology not only meets but also extends current standards in the field of synchronization, by providing a unified framework to study hybrid, nonlinear, and unidirectional quantum phenomena in a tunable opto-magno-mechanical system.

B. Nonreciprocity enabled by the synergy of the Sagnac and magnon-Kerr effects

In this section, we elucidate the physical mechanisms underlying the purely quantum nonreciprocity induced by the Sagnac and magnon-Kerr effects.

1. *Sign of the magnon-Kerr coefficient*

We mainly focus on studying the spatially uniform mode (i.e., the Kittel mode) of the ferromagnetic spin waves in a small Yttrium iron garnet (YIG) sphere. This YIG sphere, driven by a microwave field, is strongly coupled to an optomechanical cavity.

Specifically, we are interested in the spatially uniform modes, which are embodied by a large number of spins in a small-sized YIG sphere, commonly known as the Kittel mode. When including the magnetocrystalline anisotropic energy and the Zeeman energy, the Hamiltonian of a uniformly magnetized YIG sphere can be written as

$$H_m = -\int_{Vm} \mathbf{M}\cdot\mathbf{B_0}d\tau - \frac{\mu_0}{2}\int_{Vm} \mathbf{M}\cdot\mathbf{H_{an}}d\tau. \tag{S31}$$

where V_m is the volume of the YIG sphere, $\mathbf{B_0}$ depicts the applied static magnetic field, μ_0 denotes the vacuum permeability, and $\mathbf{H_{an}}$ is the anisotropic field due to the magnetocrystalline anisotropy in the YIG crystal. In addition, the magnetization of the YIG sphere is given by:

$$\mathbf{M} = (M_x, M_y, M_z) \tag{S32}$$

We can see from Eq. (S31) that the demagnetizing field leads to the demagnetization energy of the YIG sphere, and it can be omitted owing to the fact that it is a constant term.

(i) The static magnetic field is applied in the z direction, i.e., $\mathbf{B_0} = B_0 e_z$. When the crystallographic axis [100] of the YIG sphere is aligned along this static magnetic field, the resulting anisotropic field can be expressed as follows:

$$\mathbf{H_{an}} = -\frac{2K_{an}M_z}{M^2}\mathbf{e_z}, \tag{S33}$$

where the parameter M is the saturation magnetization and the parameter and K_{an} denotes the dominant first-order anisotropy constant. By bringing Eq. (S33) into Eq. (S31), the Hamiltonian of the YIG sphere obeys the following form:

$$\begin{aligned} H_m &= -\int_{Vm} \mathbf{M}\cdot B_0\mathbf{e_z}d\tau + \frac{\mu_0}{2}\int_{Vm}\mathbf{M}\cdot\frac{2K_{an}M_z}{M^2}\mathbf{e_z}d\tau \\ &= -M_z B_0 V_m + \frac{\mu_0 K_{an}M_z^2 V_m}{M^2} \\ &= -\gamma B_0 S_z + \frac{\mu_0\gamma^2 K_{an}S_z^2}{M^2 V_m}, \end{aligned} \tag{S34}$$

Note that in Eq. (S34) we have used the relation:

$$\mathbf{S} = (S_x, S_y, S_z) = \mathbf{M}V_m/\gamma, \tag{S35}$$

where the parameters $\mathbf{S}$ and γ are the macrospin operator and the gyromagnetic ratio of the YIG sphere, respectively. In order to obtain the intrinsic frequency of the magnetic mode as well as the magnetic self-kerr coefficient, it is necessary to use the Holstein-Primakoff transformation:

$$S_z = S - m^\dagger m, \tag{S36}$$

where the parameter S is the total number of spins of the YIG sphere, so that the Hamiltonian of the YIG sphere can be easily transformed into

$$\begin{aligned} H_m &= -\gamma B_0 S_z + \frac{\mu_0\gamma^2 K_{an}S_z^2}{M^2 V_m} \\ &= -\gamma B_0\left(S - m^\dagger m\right) + \frac{\mu_0\gamma^2 K_{an}\left(S - m^\dagger m\right)^2}{M^2 V_m} \\ &= \left(\gamma B_0 - \frac{2\mu_0\gamma^2 K_{an}S}{M^2 V_m}\right)m^\dagger m + \frac{\mu_0\gamma^2 K_{an}}{M^2 V_m}m^\dagger m m^\dagger m + \frac{\mu_0\gamma^2 K_{an}S^2}{M^2 V_m} - \gamma B_0 S \\ &= \omega_m m^\dagger m + \mathrm{K} m^\dagger m m^\dagger m + ... \end{aligned} \tag{S37}$$

From Eq. (S37), we show an effective frequency of the magnon mode

$$\omega_m = \gamma B_0 - \frac{2\mu_0\gamma^2 K_{an}S}{M^2 V_m}, \tag{S38}$$

which can be obtained by the comparison, and an effective magnetic self-Kerr coefficient is positive, derived as

$$\mathrm{K} = \frac{\mu_0\gamma^2 K_{an}}{M^2 V_m} > 0. \tag{S39}$$

(ii) Now, we consider the case where the crystallographic axis [110] of the YIG sphere is aligned along the static magnetic field, the anisotropic field can be obtained as:

$$\mathbf{H_{an}} = -\frac{3K_{an}M_x}{M^2}\mathbf{e_x} - \frac{9K_{an}M_y}{4M^2}\mathbf{e_y} - \frac{K_{an}M_z}{M^2}\mathbf{e_z}. \tag{S40}$$

By inserting Eq. (S40) into Eq. (S31), we can write the Hamiltonian H_m as:

$$\begin{aligned} H_m =& -\int_{V_m} \mathbf{M}\cdot B_0\mathbf{e_z}d\tau + \frac{\mu_0}{2}\int_{V_m}\mathbf{M}\cdot\left(\frac{3K_{an}M_x}{M^2}\mathbf{e_x}+\frac{9K_{an}M_y}{4M^2}\mathbf{e_y}+\frac{K_{an}M_z}{M^2}\mathbf{e_z}\right)d\tau \\ =& -M_zB_0V_m + \frac{3\mu_0K_{an}M_x^2V_m}{2M^2}+\frac{9\mu_0K_{an}M_y^2V_m}{8M^2}+\frac{\mu_0K_{an}M_z^2V_m}{2M^2} \\ =& -\gamma B_0S_z + \frac{3\mu_0\gamma^2K_{an}S_x^2}{2M^2V_m}+\frac{9\mu_0\gamma^2K_{an}S_y^2}{8M^2V_m}+\frac{\mu_0\gamma^2K_{an}S_z^2}{2M^2V_m}. \end{aligned} \tag{S41}$$

In Eq. (S41), we have used the relations:

$$M_o = \frac{S_o\gamma}{V_m}, \quad \text{for} \quad o = z, x, y, \tag{S42}$$

which is likewise used for the substitution of the parameters M_z (M_x, M_y) of Eq. (S41).

In order to obtain the magnetic mode frequency and the magnetic Kerr coefficient for the case, where the static magnetic field direction is the same as the direction of the crystallographic axis [1,1,0] of the YIG sphere, the Holstein-Primakoff transformation should also be applied into Eq. (S41). For the Hamiltonian shown in Eq. (S41), in addition to the relation $S_z = S - m^\dagger m$, we need to use the Holstein-Primakoff transformations for the parameters $S^\pm$, which are defined as:

$$S^+ = \sqrt{2S - m^\dagger m}m, \quad S^- = m^\dagger\sqrt{2S - m^\dagger m}, \tag{S43}$$

where

$$S^+ = S_x + iS_y, \quad S^- = S_x - iS_y \tag{S44}$$

are the raising and lowering macrospin operators, respectively.

In our work, the drive field leads to a considerable magnons, and the condition

$$S \gg \left\langle m^\dagger m\right\rangle \tag{S45}$$

is still satisfied owing to the fact that S is a huge number. Therefore, by approximating $S^\pm$ up to first order, it is fully reasonable for the following approximation:

$$S^+ \approx \sqrt{2S}\left[1-\frac{m^\dagger m}{4S}\right]m, \quad S^- \approx m^\dagger\sqrt{2S}\left[1-\frac{m^\dagger m}{4S}\right]. \tag{S46}$$

Since the expressions for S_x and S_y are derived from Eq. (S46), we insert S_x, S_y, and S_z into the Hamiltonian in Eq. (S41), and then using the rotating-wave approximation (RWA), the fast oscillating terms can be safely neglected. Thus, the Hamiltonian of the YIG sphere can be converted to

$$\begin{aligned} H_m =& -\gamma B_0S_z + \frac{3\mu_0\gamma^2K_{an}S_x^2}{2M^2V_m}+\frac{9\mu_0\gamma^2K_{an}S_y^2}{8M^2V_m}+\frac{\mu_0\gamma^2K_{an}S_z^2}{2M^2V_m} \\ =& \left(\gamma B_0 + \frac{13\mu_0\gamma^2K_{an}S}{8M^2V_m}\right)m^\dagger m - \frac{13\mu_0\gamma^2K_{an}}{16M^2V_m}m^\dagger mm^\dagger m \\ =& \omega_m m^\dagger m + \mathrm{K}m^\dagger mm^\dagger m + ... \end{aligned} \tag{S47}$$

Based on Eq. (S47), the effective frequency of the magnetic mode is shown as:

$$\omega_m = \gamma B_0 + \frac{13\mu_0\gamma^2K_{an}S}{8M^2V_m}, \tag{S48}$$

and the effective self-Kerr coefficient of the magnetic mode is negative, as

$$\mathrm{K} = -\frac{13\mu_0\gamma^2K_{an}}{16M^2V_m} < 0, \tag{S49}$$

According to the above discussion, we know that if the injecting direction of the magnetic field coincides with the [110] or [100] direction of the crystallographic axis of the YIG sphere, the magnetic self-Kerr coefficient is negative or positive, respectively. One can tune the system to these two situations by controlling the relative direction between the static magnetic field and the crystallization axis of the YIG sphere, thus realizing the non-reciprocity of the system.

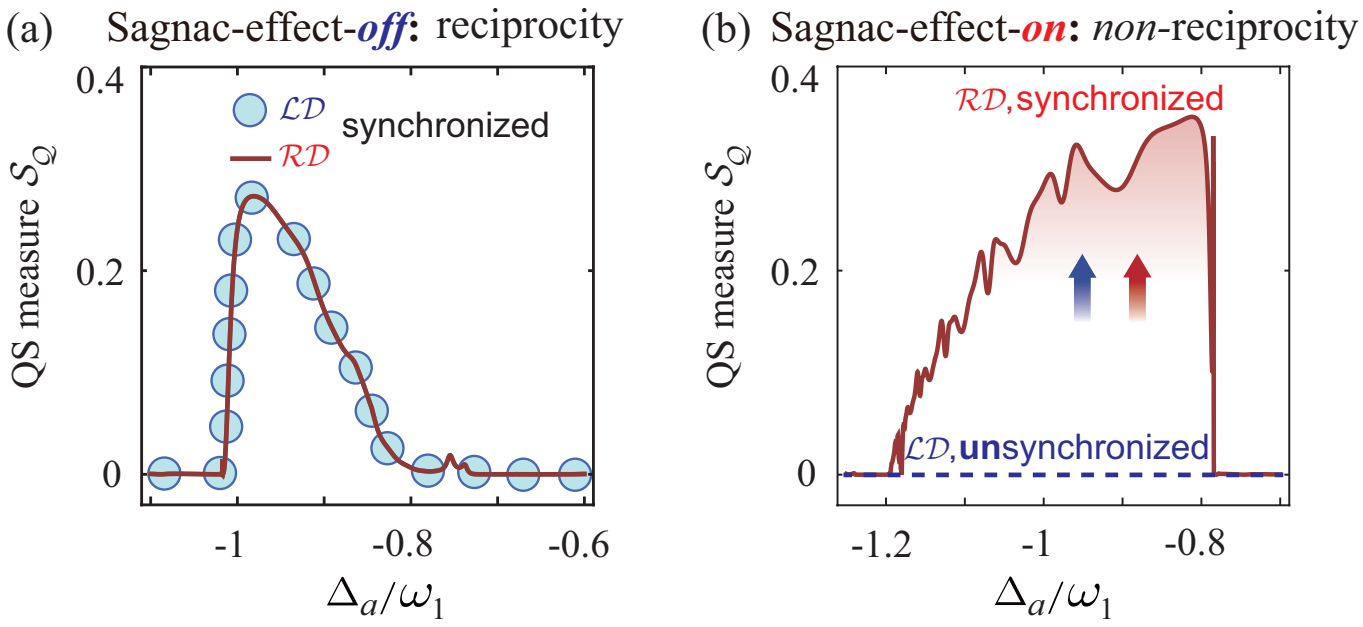

FIG. S1: For different input directions ($\mathcal{LD}$ and $\mathcal{RD}$) of the driving laser, the quantum synchronization measure $\mathcal{S}_Q$ versus the optical detuning Δ_a, when the Sagnac-effect is: (a) turned off (nonspinning, i.e., $\Omega = 0$) and (b) turned on (spinning, i.e., $\Omega \neq 0$) assuming $\Delta_m/\omega_1 = -1$. Reciprocal quantum synchronization occurs due to its independence from the injection direction of the driving laser. In contrast, nonreciprocal quantum synchronization, which is observed in the range $1.2 < \Delta_a/\omega_1 < -0.8$, arises from the system's dependence on the input directions. Here we consider the case without the magnon–Kerr nonlinearity, i.e., $\mathrm{K} = 0$.

2. *Magnon-Kerr-nonlinearity induced transition*

The magnon-Kerr effect refers to a nonlinear frequency shift of magnon modes induced by magnon-magnon interactions in a magnetically ordered material [S4]. This self-phase modulation leads to intensity-dependent magnon dynamics, analogous to the optical-Kerr effect, enabling tunable nonlinearity in hybrid quantum systems. Arising from magnetocrystalline anisotropy, this nonlinear interaction enables tunable magnon dynamics and facilitates nonperturbative phenomena such as bistability and nonreciprocal signal propagation. To explain how the Kerr-nonlinearity induced transition causes quantum nonreciprocity, we consider the *relativistic addition* of magnon frequencies into account when the magnetic field is entering from either the $\mathcal{CD}$ or $\mathcal{OD}$ wrt the crystallographic axes [110] or [100] of a YIG sphere, respectively. In light of these considerations, the magnon frequencies are different, owing to the magnetocrystalline anisotropy in the YIG sphere, thus, we predict a Kerr-nonlinearity-induced transition between the redshift and blueshift in frequency [S4], i.e.,

$$\omega_m \to \omega_m + 4\mathrm{K}N_m, \tag{S50}$$

where $N_m = |\mu|^2$ is the average magnon numbers. Evidently, the redshift and blueshift are experienced by the magnon detuning:

$$\begin{aligned}\Delta_m' &= \Delta_m - 2g_m\mathrm{Re}[\beta_1] + 4\mathrm{K}|\mu|^2,\\ &= \Delta_m - 2g_m\mathrm{Re}[\langle b_1\rangle] + 4\mathrm{K}N_m,\end{aligned} \tag{S51}$$

with Δ_m and $\beta_1 = \langle b_1\rangle$ denoting the magnon detuning without the Kerr nonlinearity and the classical part of b_1, respectively. The *relativistic origin* of the Kerr-nonlinearity-induced transition is characterized by the $4\mathrm{K}N_m$ term. Physically, the resulting negative and positive values of K are, respectively, induced by aligning the externally applied magnetic field parallel to the $\mathcal{CD}$ and $\mathcal{OD}$ of the crystallographic axes of the YIG sphere.

3. *Sagnac-Fizeau shift*

The Sagnac effect arises in rotating reference frames [S1], where counterpropagating waves traveling along a closed loop accumulate a relative phase shift proportional to the rotation rate. This relativistic interference phenomenon underpins modern gyroscopes and enables directional sensitivity in photonic and phononic systems. Inspired by the Sagnac-effect-induced nonreciprocity mechanism [S1, S2, S19], we propose the synergy of the Sagnac and magnon-Kerr effects to achieve nonreciprocal quantum synchronization.

Our original motivation is to open a new avenue for generating quantum nonreciprocity and to solve a long-standing challenge, where quantum synchronization is extremely fragile to random fabrication imperfections and thermal noise. We are the first to propose a magnon-Kerr-effect induced nonreciprocity mechanism, analogous to the Sagnac-effect-induced nonreciprocal mechanism [S1, S2, S19], to achieve our goal while simultaneously addressing these detriments. We show a detailed study on nonreciprocal quantum synchronization via the synergy of the Sagnac and magnon-Kerr effects, when the system operates in the activation regime of the self-adjustment process. (i) We reveal that the direction of an externally applied magnetic field on the magnon mode determines its Kerr nonlinearity (the magnon-Kerr effect), which offers an exciting opportunity of not only synchronizing two phonon modes but also shielding the resulted quantum synchronization against both random fabrication imperfections and thermal noise. (ii) We show that the Sagnac and magnon-Kerr effects are employed for generating nonreciprocal quantum synchronization, respectively. (iii) Unlike previous proposals naturally restricted to small-mass and/or low-dissipation regimes, our approach completely beats these limitations and achieves both noise-robust and imperfect-robust quantum resource.

Below, we show in detail how to achieve nonreciprocal quantum synchronization by employing the Sagnac effect.

The clockwise-spinning silica microsphere is driven by a laser from the left direction ($\mathcal{LD}$) or right direction ($\mathcal{RD}$) of the fibre, yielding a counterclockwise or clockwise optical mode, respectively. To explore how the Fizeau drag of light causes chirality, the *relativistic addition of velocities* is taken into account when the periphery of the spinning sphere is moving away/towards from the output/input ports. In light of these considerations, optical paths of counterpropagating light beams are different attributed to the rotation, leading to the irreversible refractive indices for a clockwise or an anti-clockwise optical mode, $\zeta \to \zeta\left[1 \pm \Omega\zeta r(\zeta^{-2}-1)/c\right]$, where the parameters ζ, Ω, r, and c are the refractive indices of materials, the spinning angular velocity of the microsphere, the sphere radius, and the light speed in vacuum, respectively. Correspondingly, an opposite Sagnac-Fizeau shift is experienced by the resonance frequency of the counterpropagating light mode [S1]:

$$\omega_a \to \omega_a + \sigma_a, \tag{S52}$$

where $\sigma_a = \pm\Omega\Lambda$ with $\Lambda = \zeta r\omega_c[1 - 1/\zeta^2 - (\lambda/\zeta)(d\zeta/d\lambda)]/c$ for the non-spinning optical frequency ω_a and the light wavelength λ. The *relativistic origin* of the Sagnac effect is characterized by the dispersion term $d\zeta/d\lambda$ [S1]. By clockwise spinning the microsphere, the resulting $\sigma_a < 0$ ($\sigma_a > 0$) corresponds to the case where the driving laser is injected from the $\mathcal{RD}$ ($\mathcal{LD}$) of the fiber. A Sagnac-Fizeau shift σ_a happens with the increase of the angular velocity Ω. Specifically, increasing the angular velocity Ω results in a linear opposite frequency shift for the counter-propagating light modes. For the same input light, due to the opposite frequency shift for the counterpropagating light modes, quantum synchronization can appear unidirectionally.

In Figs. S1(a) and S1(b), we plot the quantum-synchronization measure $\mathcal{S}_Q$ versus the optical detuning Δ_a when the system operates in the non-spinning ($\Omega = 0$) and spinning ($\Omega \neq 0$) cases. For the non-spinning (i.e., Sagnac-effect-off) case, $\mathcal{S}_Q$ is independent on the driving-laser direction [see Fig. S1(a)]; while for the spinning case (i.e., Sagnac-effect-on), it becomes different by reversing the laser direction [see Fig. S1(b)]. For example, when the quantum synchronization is created by driving the silica-microsphere cavity from the $\mathcal{RD}$, no quantum synchronization occurs by driving it from the $\mathcal{LD}$. The underlying physics can be understood as follows: in cavity optomechanics, the driving laser is scattered by the mechanical mode into the Stokes and anti-Stokes sidebands. When the cavity mode is resonant with one of the sidebands, optomechanical correlations are created. In the absence of the Sagnac effect ($\Omega = 0$), the spectral offset is due to the optomechanics-induced blueshift of the cavity mode. In the presence of the Sagnac effect ($\Omega \neq 0$), the resonance conditions for the counter-circulating light modes are modified by the opposite Sagnac shifts, resulting in the peaks symmetrically shifted for the opposite input directions.

4. *Stability analysis of the system*

We here elaborate more on the dynamical stability via the following two points: (i) stability functions [S20] and (ii) stable limit-cycle solutions [S21].

(i) Based on the Routh-Hurwitz criterion [S20], we ensure the stability of the system because all the eigenvalues of the coefficient matrix $\mathbf{A}$ have negative real parts. Therefore, our analysis begins with the determination of the eigenvalues of $\mathbf{A}$, i.e., $|\mathbf{A} - \lambda\mathbf{I}| = 0$, which results in the following characteristic equation:

$$\lambda^8 + a_1\lambda^7 + a_2\lambda^6 + a_3\lambda^5 + a_4\lambda^4 + a_5\lambda^3 + a_6\lambda^2 + a_7\lambda + a_8 = 0, \tag{S53}$$

where the parameters $a_{k=1-8}$ (i.e., $a_1, \ldots, a_8$) are the coefficients. We note that the expressions of the coefficients $a_{k=1-8}$ are quite complex, and for the sake of brevity, these expressions are not shown here. By employing $a_{k=1-8}$, a set of $k \times k$ matrices ca be constructed, i.e., θ_k for $k \leq 8$ with their entries defined as:

$$\theta_{ij} = \begin{cases} 0, & 2i - j < 0 \text{ or } 2i - j > k, \\ a_{2i-j}, & \text{otherwise.} \end{cases} \tag{S54}$$

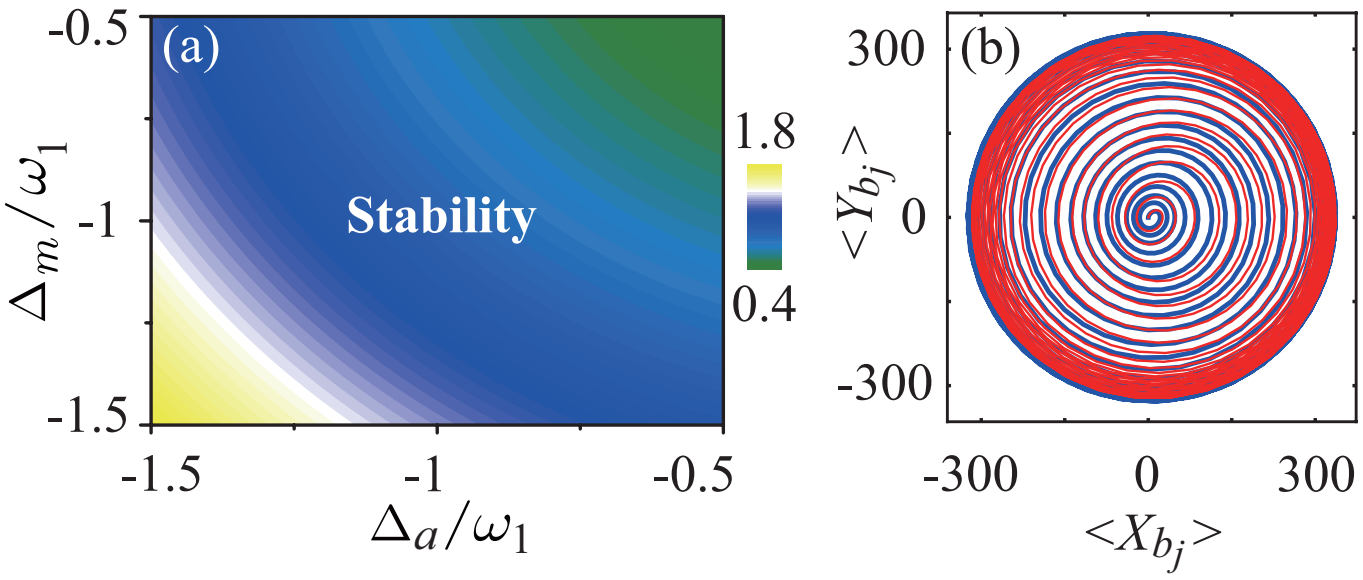

FIG. S2: (a) Stability functions θ_2 versus the optical detuning Δ_a and the magnonic detuning Δ_m. (b) Time evolution of the limit-cycle trajectories in the $\langle X_{b_j}(t)\rangle \rightleftharpoons \langle Y_{b_j}(t)\rangle$ spaces for $j = 1$ (blue solid curves) and $j = 2$ (red solid curves).

According to Eq. (S54), we see that the stability conditions are satisfied when all the determinants of the matrices θ_k are positive [S20]. Through our meticulous calculations, we found that only θ_2 is nontrivial. Specifically, we plot θ_2 as a function of the optical detuning Δ_a and the magnon detuning Δ_m, as shown in Fig. S2(a). We find that all the used parameters keep our system in a stable zone, and the system satisfies the dynamical stability around the blue-sideband resonances.

(ii) By utilizing the Routh-Hurwitz criterion [S20], all the eigenvalues of the coefficient matrix $\mathbf{A}$ are negative after a temporary evolutionary process. Hence, a stable limit-cycle solution representing a periodic oscillation exists, as shown in Fig. S2(b). We clearly see that the evolutions of $\langle X_j(t)\rangle \rightleftharpoons \langle Y_j(t)\rangle$ of the two oscillators trend to an asymptotic periodic orbit (i.e., the two limit cycles tend to be consistent). The emergence of the two consistent limit cycles indicates that the evolution of the system reaches the dynamical stability in the blue-sideband resonances.

By these two methods on elaborating the dynamical stability, we have demonstrated that all the used parameter values work in the stable zone. We highlight the enhanced stability in the nonreciprocal phase and its potential relevance for practical applications. Specifically, it not only enables one-way quantum manipulation but also contributes to the significant robustness of purely quantum effects against thermal noise and random fabrication of practical devices. These findings may be advantageous for the implementation of purely quantum behaviors in noisy or engineered quantum environments.

III. SUPPLEMENTARY DISCUSSIONS

A. Nonreciprocal quantum synchronization

Quantum synchronization describes the emergence of phase or frequency locking between interacting quantum systems, despite intrinsic quantum fluctuations [S3]. It extends classical synchronization into the quantum regime, revealing nontrivial correlations in the dynamics of coupled oscillators, spins, or fields. Unlike its classical counterpart, quantum synchronization manifests through correlations in quantum observables and is constrained by quantum noise and noncommutativity, offering a route to controlling collective quantum dynamics.

The burgeoning field of nonreciprocal physics has captured widespread interest across classical and quantum disciplines. Remarkably, while numerous demonstrations have illuminated its principles in diverse contexts, a conspicuous gap remains unexplored within the realm of quantum resources: quantum synchronization. Here we bridge this critical void by attaining nonreciprocal quantum synchronization, unveiling its counterintuitive resilience against device imperfections and thermal noise. Through the utilization of magnetic-Kerr nonlinearity, we achieve synchronization of two vibrations along a specified direction of the magnetic field while maintaining desynchronization along the orthogonal direction, thereby establishing a novel unidirectional quantum synchronization paradigm. In contrast to prior proposals constrained by high-quality and small-mass considerations, our methodology confers robustness against such limitations, thus presenting a notable advancement in quantum synchronization. Significantly, our approach exhibits a remarkable resurgence of synchronization resilience against thermal

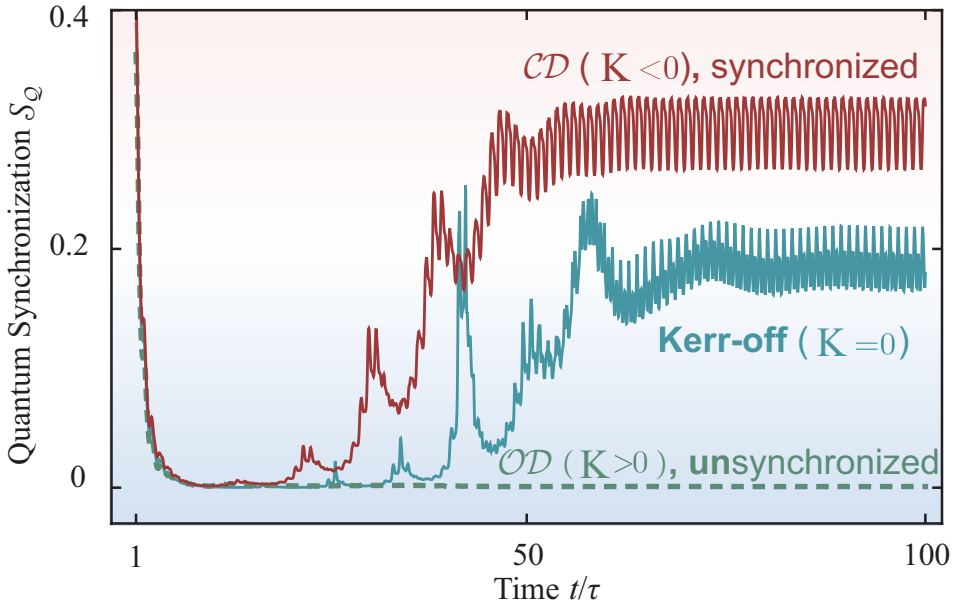

FIG. S3: Quantum synchronization measure $\mathcal{S}_Q$ versus time t, when the magnetic field is injected from a chosen direction ($\mathcal{CD}$) and the other direction ($\mathcal{OD}$). A one-way quantum synchronization appears for different injecting directions of the external magnetic field, yielding a redshift or blueshift in the magnon detuning, .

noise in real-world applications, a phenomenon unprecedented in extant literature. This study lays a cornerstone for fortifying and manipulating delicate quantum phenomena through the utilization of a spectrum of nonreciprocal devices. Such endeavors promise to facilitate the realization of quantum resources that are both impervious to imperfections and resilient to noise, thereby paving the way for advanced quantum technologies.

In this section, we investigate unidirectional quantum synchronization using a hybrid quantum framework. This framework entails a silica microsphere, serving as an optomechanical cavity, in conjunction with a YIG microsphere, acting as a magnomechanical cavity. These entities are simply linked through a direct physical contact, enabling coherent coupling between them. Concretely, we first study the unidirectional quantum synchronization of two phonon modes, which is dependent on the direction of the magnetic field. We then show its tolerance against the device imperfections by employing the magnon-Kerr effect. By analyzing the robustness of quantum synchronization against thermal noise in a highly imperfect devices, we can confirm the action of the magnon-Kerr nonlinearity on the revival and enhancement of quantum synchronization.

1. *Nonreciprocity in quantum synchronization*

Nonreciprocal quantum synchronization can be easily induced in a hybrid quantum platform, consisting of a silica microsphere in combination with a YIG microsphere, coherently coupling to each other via a straightway physical contact. The mechanical vibration in the silica (YIG) microsphere is explored by the radiation-pressure (magnetostrictive) force through the circulating-optical fields (microwave-driven magnons). The introduced magnon-Kerr nonlinearity plays a critical role in the creation of nonreciprocal quantum synchronization. Below, we study how the magnon-Kerr nonlinearity affects the generation of one-way quantum synchronization. Specifically, we detailedly study the dependence of the nonreciprocal quantum synchronization on the system parameters, when the system operates in both the magnon-Kerr-off and -on regimes.

To this end, we plot in Fig. S3 the quantum synchronization measure $\mathcal{S}_Q$ as a function of the evolution time t when the system operates in the $\mathcal{CD}$ ($\mathrm{K}/\omega_1 = -2\times10^{-5}$), magnon-Kerr-off ($\mathrm{K} = 0$), and $\mathcal{OD}$ ($\mathrm{K}/\omega_1 = 2\times10^{-5}$) cases. We see that for the $\mathcal{CD}$ and standard cases, the quantum synchronization measure becomes nonzero $\mathcal{S}_Q > 0$ around $t/\tau > 50$, which indicates the quantum synchronization of two phonon modes. In a stark contrast to this, a zero value of $\mathcal{S}_Q$ appears in the $\mathcal{OD}$ case, which implies to no quantum synchronization of the two phonon modes. These results demonstrate that a fundamentally different nonreciprocity of quantum resources can be accomplished, which is otherwise unattainable in conventional schemes.

In particular, the quantum synchronization measure $\mathcal{S}_Q$ in the $\mathcal{CD}$ case is larger than both standard and $\mathcal{OD}$ cases. This is because the introduced magnon-Kerr nonlinearity enabled in the hybrid quantum system can be modulated by tuning the magnon-Kerr nonlinearity, which is achieved by changing the direction of the magnetic field. The maximal quantum synchronization emerges, corresponding to a strong magnon-Kerr nonlinearity. Physically, the magnetic field entering from the $\mathcal{CD}$ yields a blue

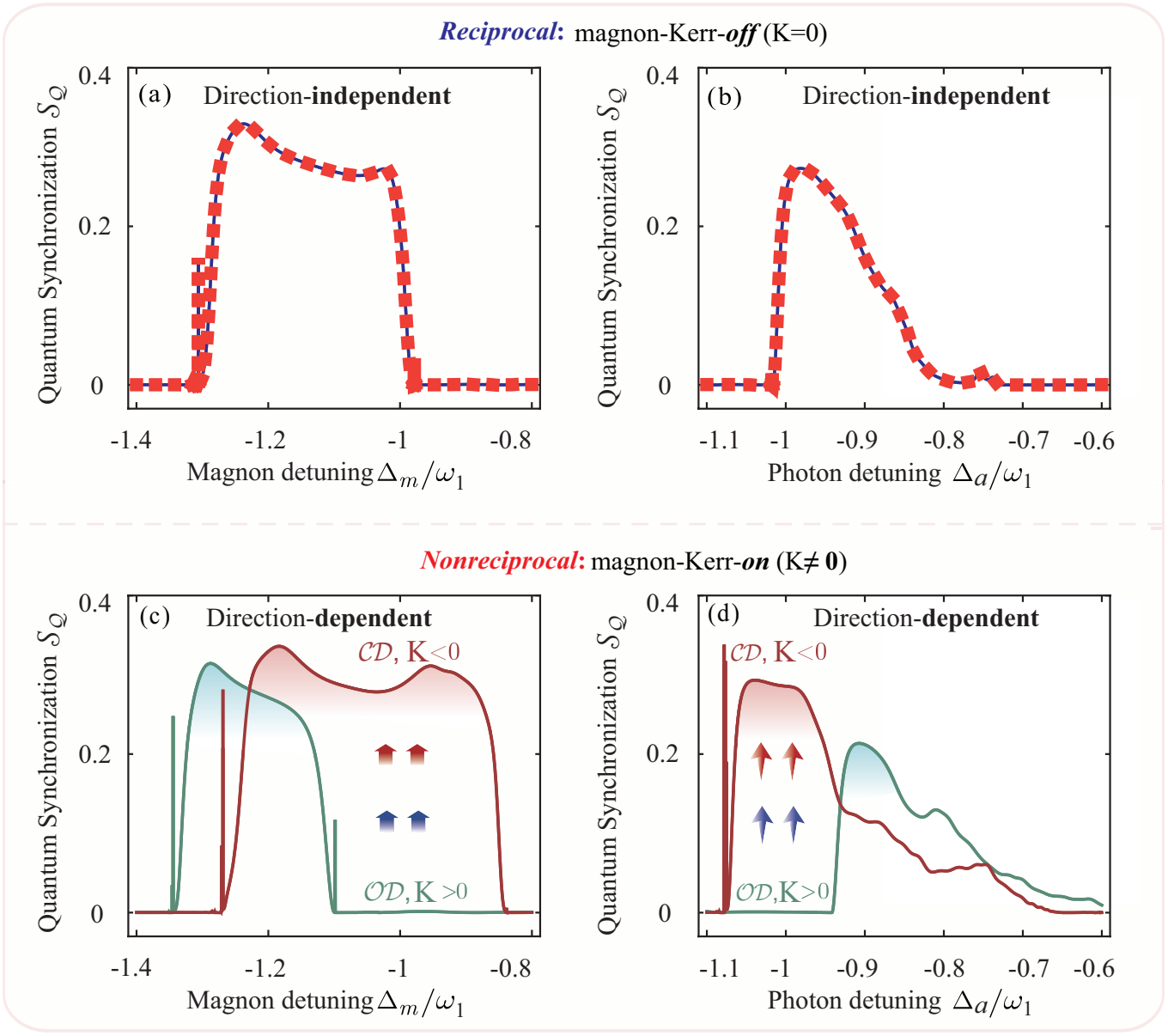

FIG. S4: In the magnon-Kerr-off regime, quantum synchronization measure $\mathcal{S}_Q$ versus (a) the magnon detuning Δ_m and (b) the optical detuning Δ_a. A reciprocity of quantum synchronization happens due to the independence on the injecting direction of the magnetic field. In the magnon-Kerr-on regime, $\mathcal{S}_Q$ versus (c) Δ_m and (d) Δ_a for the $\mathcal{CD}$ (K/$\omega_1 = -2\times10^{-5}$), and $\mathcal{OD}$ (K/$\omega_1 = 2\times10^{-5}$) cases. A unidirectional quantum synchronization occurs around $\Delta_m/\omega_1 \approx -1$ and $\Delta_a/\omega_1 \approx -1$, because of the dependence on the injecting magnetic-field direction.

shift of the magnon detuning, whereas when injected from the $\mathcal{OD}$ leads to an opposite shift. This can be further demonstrated by studying the dependence of $\mathcal{S}_Q(t)$ on t when the magnetic field enters from the $\mathcal{CD}$ or $\mathcal{OD}$. For the $\mathcal{CD}$ case, an efficient quantum synchronization appears; while for the $\mathcal{OD}$ case, *no* quantum synchronization occurs. This demonstrates the emergence of unidirectional quantum synchronization, which has no correspondence to the previously established demonstrations on quantum synchronization.

To better comprehend this counterintuitive unidirectional quantum behavior, we plot the quantum synchronization measure $\mathcal{S}_Q$ as a function of the detunings Δ_m and Δ_a, in both the magnon-Kerr-off and magnon-Kerr-on regimes, as shown in Figs. S4(a,b) and S4(c,d), respectively. For the magnon-Kerr-off regime (i.e., K = 0), the quantum synchronization measure $\mathcal{S}_Q$ is independent of the direction of the injected magnetic field, and this means the reciprocity of quantum synchronization, as shown in Figs. S4(a) and S4(b). However, by introduction the magnon-Kerr nonlinearity (i.e., the magnon-Kerr-on regime, K $\neq$ 0), the quantum synchronization measure $\mathcal{S}_Q$ becomes fundamentally different once switching the magnetic-field direction, which indicates the nonreciprocity, as shown in Figs. S4(c) and S4(d).

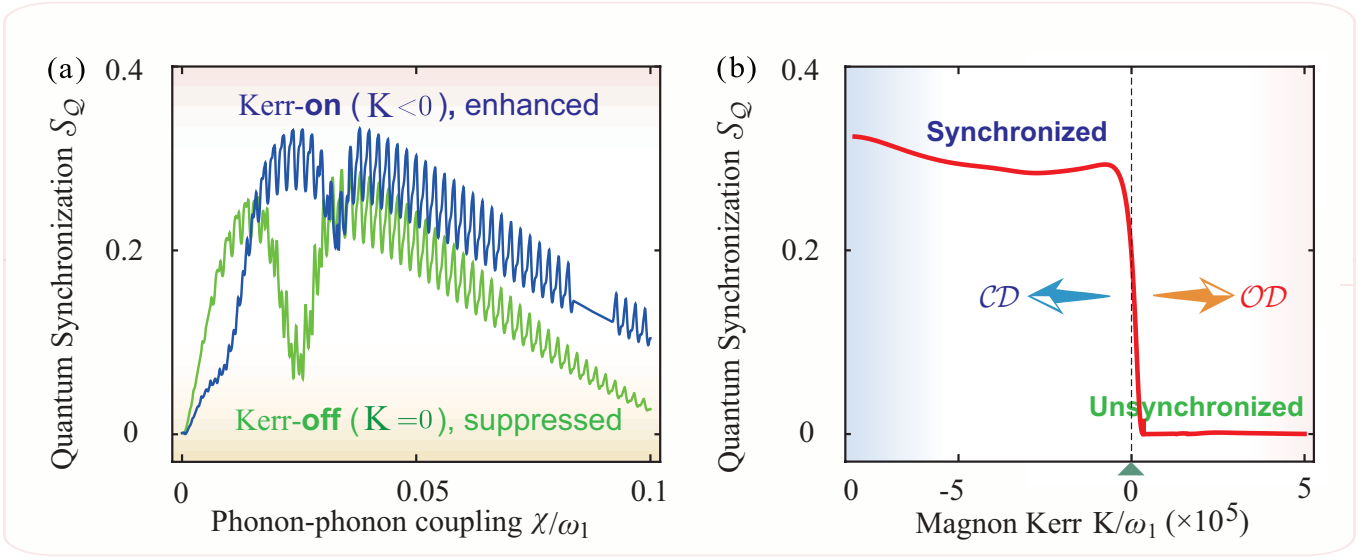

FIG. S5: (a) Quantum synchronization measure $\mathcal{S}_Q$ versus the phonon-phonon coupling strength χ, in the presence of the magnon-Kerr nonlinearity (i.e., $\mathrm{K}/\omega_1 \neq 0$), assuming that the externally injected magnetic field enters from the $\mathcal{CD}$ ($\mathrm{K}/\omega_1 = -2\times10^{-5}$) and $\mathcal{OD}$ ($\mathrm{K}/\omega_1 = 2\times10^{-5}$). (b) Quantum synchronization measure $\mathcal{S}_Q$ versus the magnon-Kerr nonlinearity strength K. Here we assume $\Delta_m/\omega_1 = -1$ and $\Delta_a/\omega_1 = -1$.

Concretely, we find that for

$$-1.1 \lesssim \Delta_m/\omega_1 \lesssim -0.8, \tag{S55}$$

or

$$-1.1 \lesssim \Delta_a/\omega_1 \lesssim -0.9, \tag{S56}$$

quantum synchronization does not happen in the $\mathcal{OD}$, while it is generated in the $\mathcal{CD}$. In addition, the maximal quantum synchronization can be observed at the blue-sideband resonances, i.e.,

$$\Delta_m \approx -\omega_1, \quad \text{and} \quad \Delta_a \approx -\omega_1. \tag{S57}$$

This indicates that by employing the magnon-Kerr effect, quantum nonreciprocity can emerge. Our findings pave a route to constructing a general nonreciprocal quantum device.

Now, we study the dependence of quantum synchronization on the phonon-phonon interaction by plotting the quantum synchronization measure $\mathcal{S}_Q$ as a function of the phonon-phonon coupling strength χ, when the system operates in the magnon-Kerr-on ($\mathcal{CD}$, $\mathrm{K}/\omega_1 = -2\times10^{-5}$) and magnon-Kerr-off ($\mathrm{K} = 0$) regimes, as shown in Fig. S5(a). It is clearly shown that the quantum synchronization is suppressed in the magnon-Kerr-off regime, but enhanced in the magnon-Kerr-on regime, giving rise to an enhancement of the quantum behavior.

In addition, we display the effect of the magnon-Kerr nonlinearity on quantum synchronization by plotting the quantum synchronization measure $\mathcal{S}_Q$ as a function of the magnon-Kerr nonlinearity strength K, as shown in Fig. S5(b). We reveal in Fig. S5(b) that, for the $\mathcal{OD}$ case, i.e.,

$$\mathrm{K} > 0, \tag{S58}$$

no quantum synchronization of the two phonon modes occurs, i.e.,

$$\mathcal{S}_Q = 0; \tag{S59}$$

while for the $\mathcal{CD}$ case, i.e.,

$$\mathrm{K} < 0, \tag{S60}$$

a significant quantum synchronization appears, i.e.,

$$\mathcal{S}_Q > 0. \tag{S61}$$

This is contributed to the fact that the system possesses a shift of detuning, as a result of the magnon-Kerr nonlinearity, and it destroys the quantum resource. In contrast, when we choose a proper direction of the magnetic field ($\mathcal{CD}$, i.e., K < 0), the optomechanical and magnonmechanical vibrations become synchronized efficiently.

We also see from Fig. S5(b) that an optimal value of the quantum synchronization measure locates around the blue-sideband resonance, i.e., $\Delta_{m(a)} \approx -\omega_1$, for a proper value of the magnon-Kerr strength. Additionally, the quantum synchronization of the two phonon modes is completely destroyed, i.e., $\mathcal{S}_Q = 0$ in the $\mathcal{OD}$ case (i.e., K > 0), which corresponds to the vanishment of quantum synchronization. Hence, it is possible to switch a quantum device between unsynchronization and synchronization of the two phonon modes by simply tuning the magnon-Kerr strength.

2. *Imperfection-tolerant quantum synchronization*

TABLE II: **Classification of Large Mass and High Dissipation as Random Fabrication Imperfections in Quantum Physics**

Property	**Random Fabrication Imperfection?**	**Scientific Justification**
Large mass	Yes	Often determined by design, but unintended variations in geometry, etching depth, or material deposition during fabrication can randomly increase the effective mass of quantum components.
High dissipation	Yes	Predominantly caused by uncontrollable factors such as microscopic defects, interface roughness, and residual impurities introduced stochastically during imperfect nanofabrication processes, leading to decoherence and energy loss.

In quantum physics, large mass and high dissipation are frequently manifestations of random fabrication imperfections in quantum devices. Deviations in etching depth, layer uniformity, or material composition can lead to increased inertial mass; while microscopic defects, impurities, and surface roughness introduce unwanted dissipation, as shown in Tab. II. Such imperfections can significantly impair quantum coherence and quantum control, highlighting the imperative for ultrahigh-precision shielding in scalable quantum technologies.

As is well-known, fragile quantum resources can be easily destroyed by detrimental imperfections (e.g., large-mass and/or high-loss) in practical quantum devices. Nevertheless, our approach overcomes this outstanding limitation, and paves a feasible strategy to shielding fragile quantum resources from the device detriments, enabling the construction of imperfection-free unidirectional quantum synchronization devices. Physically, the resulting imperfection-tolerant quantum synchronization is a consequence of the improved resilience of the resonator rather than a better frequency matching between the two phonon modes.

To demonstrate this counterintuitive imperfection-tolerant finding, we display the quantum synchronization measure $\mathcal{S}_Q$ as functions of the mass ratio m_j/m_0 and the phononic decays γ_j/ω_1 of the two resonators, in the magnon-Kerr-off (i.e., K = 0) and magnon-Kerr-on ($\mathcal{CD}$, i.e., $\mathrm{K}/\omega_1 = -2 \times 10^{-5}$) regimes [see Fig. 3(a,b) of the main text]. We find that in the absence of the magnon-Kerr nonlinearity (K = 0), quantum synchronization is suppressed in a wide mass-ratio range, and the suppression range of quantum synchronization becomes much wider for a larger value of the mass ratio m_j/m_0. For example, we show that the suppression effect of quantum synchronization is observed for a finite mass-ratio range, and that the range for the magnon-Kerr-off regime (K = 0) is wider than that for the magnon-Kerr-on regime (K < 0). By introducing the magnon-Kerr nonlinearity, we see that the the opto-vibrational and magno-vibrational modes are synchronized irrespective of the value of the mass ratio m_j/m_0 for the $\mathcal{CD}$ of the magnetic field. This is attributed to the magnon-Kerr nonlinearity effect, which dramatically improves the resilience of the resonator. These results confirm that the two phonon modes can be effectively synchronized utilizing the magnon-Kerr nonlinearity even when quantum synchronization is fully destroyed in the magnon-Kerr-off case (i.e., K = 0). By employing the power of the magnon-Kerr nonlinearity, quantum synchronization can be switched from significantly suppressed, or even fully destroyed, to highly synchronized. Our findings indicate that the introduced magnon-Kerr-nonlinearity magnetism can be used for enhancing quantum synchronization, and especially, the work window of the magnon-Kerr nonlinearity becomes wider for a larger value of the mass ratio of the resonators.

In addition, we find that when turning off the magnon-Kerr nonlinearity (i.e., in the magnon-Kerr-off regime), the suppression effect appears for quantum synchronization in a wide range of the phonon decays, and its suppression range becomes much wider for a larger value of the phononic decay, as shown in Figs. S6 and S7. Specifically, we find that in a finite mechanical decay range, the quantum-synchronization suppression happens, and that the suppression range for the magnon-Kerr-off regime (i.e., K = 0) is wider than that for the magnon-Kerr-on regime (i.e., K < 0). By introducing the magnon-Kerr nonlinearity (i.e., in the magnon-Kerr-on regime), the the opto-mechanical and magnon-mechanical vibrations are synchronized regardless of the value of the phononic decay rates, as shown in Figs. S6 and S7. Our investigation unveils a striking phenomenon wherein the two phonon modes achieve remarkable synchronization, courtesy of the magnon-Kerr effect. Notably, this quantum synchronization

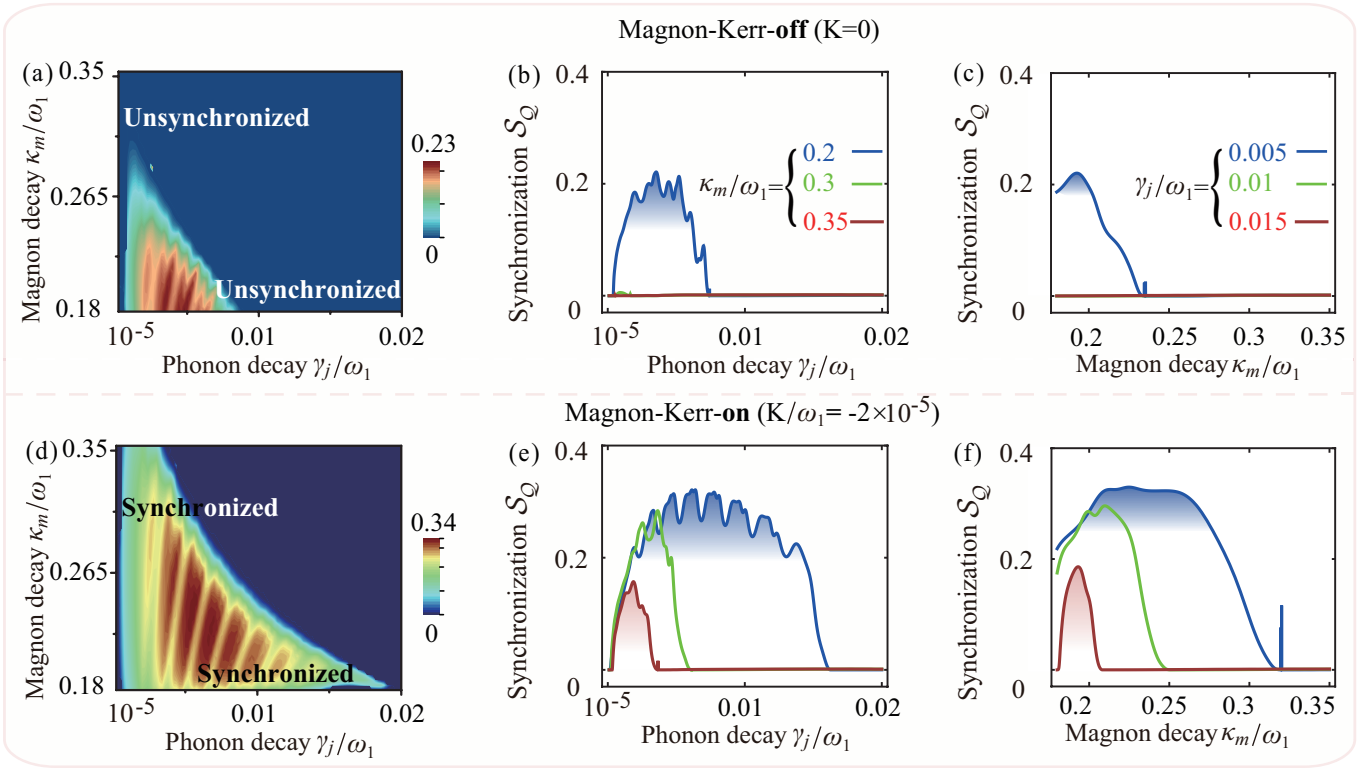

FIG. S6: (a,d) Quantum synchronization measure $\mathcal{S}_Q$ versus the mechanical decay rate γ_j and the magnon decay rate κ_m in (a) the magnon-Kerr-off and (d) Kerr-on cases. (b,e) Quantum synchronization measure $\mathcal{S}_Q$ versus the phononic damping rate γ_j in (b) the magnon-Kerr-off and (e) Kerr-on cases. (c,f) Quantum synchronization measure $\mathcal{S}_Q$ versus the magnon decay rate κ_m in (c) the magnon-Kerr-off and (f) Kerr-on cases.

persists even in scenarios where quantum synchronization faces complete disruption, as evidenced in the absence of magnon-Kerr nonlinearity. We further reveal that by introducing the magnon-Kerr nonlinearity effect, quantum synchronization of the two phonon modes becomes effectively synchronized from significantly suppressed (or even fully destroyed), as detailed in Figs. S6 and S7. These results suggest that the novel type of the magnon-Kerr-induced magnetism introduced here holds promise for augmenting quantum synchronization. Notably, the operational range of the magnon-Kerr nonlinearity appears to broaden with the increased decay rates of the resonators, offering intriguing prospects for further exploration.

In particular, we have demonstrated that in the absence of the magnon-Kerr nonlinearity, quantum synchronization is deteriorated with the increase of the mass ratio; while by employing the magnon-Kerr effect, it becomes significantly enhanced, which paves a route to the generation of mass-free quantum resources, as shown in Fig. 3(a) of the main text. This finding solidifies the notion that the magnon-Kerr effect facilitates remarkable quantum synchronization between two phonon modes, even in scenarios where quantum synchronization would otherwise be completely disrupted in the absence of the magnon-Kerr nonlinearity. For further demonstrating this point, the dependence of quantum synchronization on the resonator mass can be clearly seen by operating the system in the magnon-Kerr-off and magnon-Kerr-on cases. We find that in the magnetic-Kerr-off regime (K = 0), the two phonon modes are unsynchronized ($\mathcal{S}_Q = 0$) when the mass ratio $\rho = m_j/m_0 > 1$. In stark contrast to this, the two phonon modes become effectively synchronized ($\mathcal{S}_Q > 0$) in the magnetic-Kerr-on regime (K < 0). Physically, the reduction of quantum synchronization due to the decrease in the magnon-phonon coupling with increasing the resonator mass; while it can be considerably compensated or even amplified, contributed from the introduction of the magnon-Kerr nonlinearity effect. Physically, injecting the magnetic field from the $\mathcal{CD}$ ($\mathcal{OD}$) yields the symmetric (asymmetric) coupling, indicating the enhancement (degradation) in the resonator resilience. It indicates that, in general, by simply employing the magnon-Kerr mechanism, quantum synchronization can be nearly robust against both mass and damping of practical devices.

In addition, we find that in the nondegenerate-resonator case (i.e., $\omega_1 \neq \omega_2$), the quantum synchronization may be slightly degraded. We explain this synchronization-degradation phenomenon based on the following fact. The quantum synchronization effect exists within a very narrow frequency-detuning window of the two resonator, and therefore, within this window, the mismatch of the phononic resonance frequencies is the dominating factor for the synchronization-generation performance. By using the magnon-Kerr nonlinearity, the combination effect of the original light-motion couplings and the introduced magnon-Kerr mechanism governs the generation of quantum synchronization, and hence the quantum combinated effect can improve the

quantum synchronization of the opto-mechanical and magnon-mechanical motions.

The phonon modes are thermalized by their thermal baths through the mechanical dissipation channels, and thermal noises can destroy fragile quantum responses in practical devices. In particular, the magnon numbers are decreased by its damping through the magnon dissipation channels, and as a result, a high magnon decay rate can destroy fragile quantum behavior in highly imperfect setups. Below, we study the dependence of quantum synchronization on the mechanical decay rate γ_j and the magnon decay rate κ_m, when the system operates in both magnon-Kerr-off and -on regimes.

To elucidate this aspect, we display in Figs. S6(a) and S6(d) the quantum synchronization measure $\mathcal{S}_Q$ as functions of the mechanical decay rate γ_j and the magnon decay rate κ_m, when the system undergoes the magnon-Kerr-off and magnon-Kerr-on cases. Specifically, we see that when increasing either mechanical and magnon decay rates, a strong suppression effect of quantum synchronization occurs, and that when $\kappa_m/\omega_1 > 0.27$ or $\gamma_j/\omega_1 > 0.007$, the quantum synchronization becomes completely vanished. In particular, we reveal that the suppression effect of quantum synchronization in the magnon-Kerr-off regime (i.e., $\mathrm{K} = 0$) is much larger than that in the magnon-Kerr-on regime (i.e., $\mathrm{K} < 0$). This indicates that by employing the magnon-Kerr nonlinearity, we can protect the quantum synchronization of the two phonon modes from both phonon and magnon decay rates. These findings emphasize the ability of the magnon-Kerr effect to synchronize the two vibrations, even in scenarios where quantum synchronization is entirely disrupted in the absence of magnetic-Kerr interaction. Utilizing the potency of magnon-Kerr nonlinearity, quantum synchronization ($\mathcal{S}_Q$) can transition from substantial suppression, or even complete disruption, to full synchronization. These outcomes suggest that the introduced magnon-Kerr magnetism holds promise for augmenting quantum synchronization. Notably, the operational scope of magnon-Kerr nonlinearity expands with increasing decay rate of the mechanical resonator.

For further illustrating the above findings, we plot the quantum synchronization measure $\mathcal{S}_Q$ as a function of the mechanical decay rate γ_j, when the system operates in both the magnon-Kerr-off (see green solid curves) and -on (yellow solid curves) regimes, as shown in Figs. S6(b) and S6(e). We find that the values of the quantum synchronization measure $\mathcal{S}_Q$ increase with the decrease of the mechanical decay rate γ_j. This is because the thermal-noise-exchange rates between the mechanical resonators and their heat baths are much slower for a smaller value of the decay rate γ_j, and it is good for protecting fragile quantum resources from environmental thermal perturbations. This indicates that a high Q-factor resonator holds promise for generating a robust quantum synchronization. In addition, Figs. S6(b) and S6(e) show

$$\mathcal{S}_Q^{\mathrm{on}} > \mathcal{S}_Q^{\mathrm{off}} \tag{S62}$$

because the magnon-Kerr strength is set as

$$\mathrm{K}/\omega_1 < 0, \tag{S63}$$

corresponding to turning on the magnon Kerr, and this means that the quantum synchronization in the magnon-Kerr-on case is stronger than that in the case without the magnon-Kerr nonlinearity ($\mathrm{K} = 0$).

In particular, we observe that in the magnetic-Kerr-off regime ($\mathrm{K} = 0$), the two phonon modes are unsynchronized ($\mathcal{S}_Q = 0$) with the increase of γ_j; in stark contrast to this, they become effectively synchronized ($\mathcal{S}_Q > 0$) in the magnon-Kerr-on regime ($\mathrm{K} < 0$). Physically, the decrement in quantum synchronization arises from the diminishing effective interaction between magnons and phonons as phononic damping rates increase. However, this reduction can be substantially mitigated, or even amplified, by the inclusion of the magnon-Kerr effect. This suggests that, broadly speaking, the mere utilization of the magnetic-Kerr mechanism renders quantum synchronization nearly impervious to damping effects in practical devices.

In addition, we plot in Figs. S6(c) and S6(f) the quantum synchronization measure $\mathcal{S}_Q$ versus the magnon damping rate κ_m, in both the magnon-Kerr-off and magnon-Kerr-on regimes. We see that the decrease in the quantum synchronization measure $\mathcal{S}_Q$ observes with the increase of the magnon decay rate κ_m. This is because the excitation-exchange rates are much faster for a larger value of the magnon decay rate κ_m, and it is good for shedding fragile quantum resources from the magnon loss in practical devices, indicating that a high Q-factor magnon setup can hold promise for generating a highly robust quantum synchronization. It shows in Figs. S6(c) and S6(f) the result of $\mathcal{S}_Q^{\mathrm{on}} > \mathcal{S}_Q^{\mathrm{off}}$, owing to the fact that the magnon-Kerr strength $\mathrm{K}/\omega_1 < 0$ is set, thus quantum synchronization in the magnon-Kerr-on regime is stronger than that in the magnon-Kerr-off regime. Furthermore, we elucidate that within the magnetic-Kerr-off regime ($\mathrm{K} = 0$), the two vibrations exhibit desynchronized behavior ($\mathcal{S}_Q = 0$), whereas in stark contrast, they demonstrate synchronization ($\mathcal{S}_Q > 0$) within the magnon-Kerr-on regime ($\mathrm{K} < 0$). This is because the attenuation of quantum synchronization stems from a reduction in magnon-phonon interaction as magnetic damping rates increase. However, this diminishment in magnon-phonon coupling strength can be substantially counteracted, or even intensified, by the incorporation of the magnetic-Kerr effect. This implies that, broadly speaking, the mere utilization of the magnetic-Kerr mechanism can confer near robustness against damping in quantum synchronization.

Now, we show how to employ the magnon-Kerr nonlinearity effect to accomplish the robustness of quantum synchronization against the device imperfection, by plotting the quantum synchronization measure $\mathcal{S}_Q$ as functions of the mechanical γ_j (magnetic κ_m, optical κ_a) decays and the magnon-Kerr nonlinearity strength K, as shown in Fig. S7.

Firstly, to comprehend the counterintuitive phenomena, we show the quantum synchronization measure $\mathcal{S}_Q$ versus the mechanical decay rate γ_j and the magnon-Kerr nonlinearity K in Fig. S7(a). We see that in the absence of the magnon-Kerr

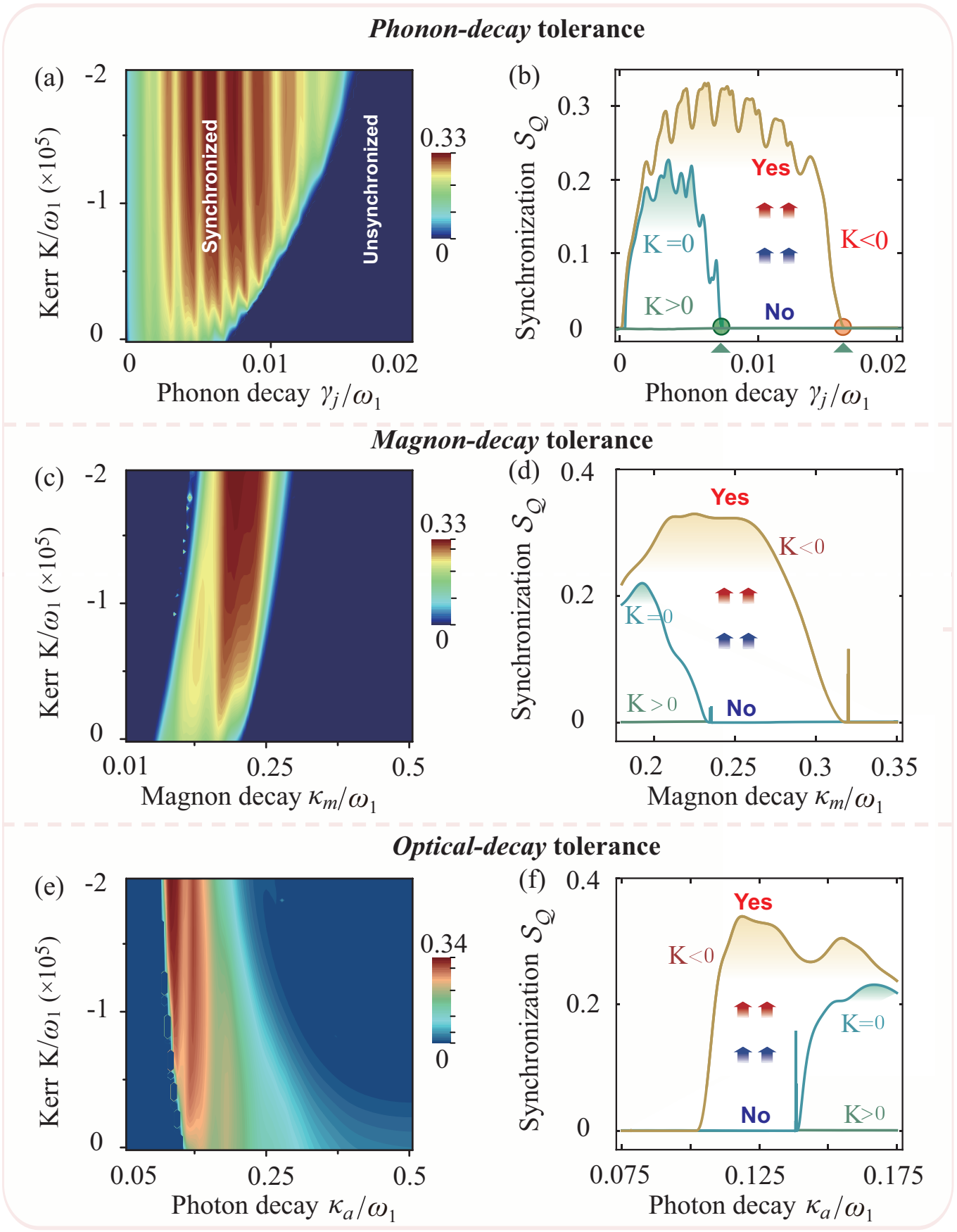

FIG. S7: (a) Quantum synchronization measure $\mathcal{S}_Q$ versus the mechanical decay rates γ_j and the magnon-Kerr strength K. (b) Quantum synchronization measure $\mathcal{S}_Q$ versus the mechanical decay rate γ_j when the magnon-Kerr strength K = 0, < 0, > 0. (c) Quantum synchronization measure $\mathcal{S}_Q$ versus the magnetic decay rate κ_m and the magnetic-Kerr strength K. (d) Quantum synchronization measure $\mathcal{S}_Q$ versus the magnetic decay rate κ_m when the magnon-Kerr strength K = 0, < 0, > 0. (e) Quantum synchronization measure $\mathcal{S}_Q$ versus the optical decay rate κ_a and the magnon-Kerr strength K. (f) Quantum synchronization measure $\mathcal{S}_Q$ versus the optical decay rate κ_m when the magnetic-kerr strength K = 0, < 0, > 0.

effect (i.e., K = 0), the opto- and magnon-mechanical vibrations are unsynchronized (i.e., $\mathcal{S}_Q = 0$), when $\gamma_j/\omega_1 > 0.007$. In the presence of the magnetic-Kerr effect (i.e., K < 0), a strong quantum synchronization can be achieved regardless the mechanical decay. Moreover, this counterintuitive finding can be confirmed by plotting the quantum synchronization measure $\mathcal{S}_Q$ versus the mechanical γ_j when the system works in both the magnon-Kerr-off and -on cases. Here, we see that, in the magnetic-Kerr-off case, no quantum synchronization emerges between the opto- and magnon-mechanical vibrations, i.e., $\mathcal{S}_Q = 0$ (see the solid curves); while by introducing the magnon-Kerr effect (i.e., K < 0), these two phonon modes can be effectively synchronized in the quantum regime, as shown in Fig. S7(b).

For comprehending these counterintuitive phenomena, we show the quantum synchronization measure $\mathcal{S}_Q$ versus the rescaled magnon-field decay rate κ_m/ω_1 and the magnon-Kerr nonlinearity K, as shown in Fig. S7(c). To further demonstrate this, in Fig. S7(d), the quantum synchronization measure $\mathcal{S}_Q$ is plotted as a function of the rescaled magnon-field decay rate κ_m/ω_1, when the system works in both the magnon-Kerr-off and -on regimes. Here, we observe that in the magnon-Kerr-off regime, the two phonon modes are unsynchronized, i.e., $\mathcal{S}_Q = 0$ (see the solid curves) when $\kappa_m/\omega_1 > 0.24$; whereas switching to the magnon-Kerr-on case (i.e., K < 0), the quantum synchronization can be realized when the system is in the resolved-sideband regime. In particular, the optimal working parameter of the cavity-field decay rate κ_m (corresponding to the maximum value of the quantum synchronization measure $\mathcal{S}_Q$) is around $\kappa_m/\omega_1 \approx 0.25$.

In addition, employing the magnon-Kerr effect effect can give rise to a counterintuitive robustness against the optical damping. To illustrate this, we plot the quantum synchronization measure $\mathcal{S}_Q$ as functions of the optical decay κ_a and the magnon-Kerr nonlinearity strength K, as shown in Fig. S7(e). We can see that in the magnetic-Kerr-off case, the two mechanical modes are unsynchronized when $\kappa_a/\omega_1 < 0.14$; while they become strongly synchronized once using the magnon-Kerr nonlinearity (i.e., K < 0), which is fully beyond the synchronization limitation from the photon decay rate. In particular, we plot the quantum synchronization measure $\mathcal{S}_Q$ versus the photon decay rate κ_a, as shown in Fig. S7(f). It clearly shows that when the system is in the resolved-sideband regime (i.e., $\kappa_a \ll \omega_m$), the two phonon modes are unsynchronized without the magnon-Kerr nonlinearity, but synchronized by introducing this Kerr mechanism. In the magnon-Kerr-on regime, the optimal working parameter of κ_a (corresponding to the maximum value of $\mathcal{S}_Q$) is around $\kappa_a/\omega_1 \approx 0.125$, corresponding to no quantum synchronization $\mathcal{S}_Q = 0$ for the magnon-Kerr-off regime.

In a word, we demonstrated the quantum synchronization of two phonon modes through the magnon-Kerr effect, even in scenarios where quantum synchronization is typically disrupted in the magnetic-Kerr-off case. Leveraging the magnon-Kerr nonlinearity, we observe a remarkable transition in quantum synchronization ($\mathcal{S}_Q$), from a state of significant suppression or complete destruction to full synchronization. Our findings underscore the potential of magnon-Kerr magnetism in bolstering quantum synchronization, particularly highlighting its efficacy in widening the operational range of the magnon-Kerr-induced nonlinearity, especially evident with higher decay rates of the mechanical resonators.

3. *Noise-robust quantum synchronization*

The detrimental effects of thermal noises on delicate quantum resources are well-documented in practical devices. Here, we propose a novel approach, leveraging magnon-Kerr magnetism, to shield fragile quantum resources from environmental thermal perturbations. Our method demonstrates a substantial enhancement in the noise tolerance of quantum synchronization, offering promising avenues for robust quantum information processing amidst challenging thermal environments. We have demonstrated that compared to the magnon-Kerr-effect-off case, the effective mechanical dissipation becomes much smaller in the $\mathcal{CD}$ case, giving rise to improving the resilience of the resonator; while it becomes much larger in the $\mathcal{OD}$ case, resulting in reducing this resilience. Physically, the noise-exchange rates between phonon modes and their effective heat baths are much slower for a smaller value of the effective decay rate, and it is beneficial for protecting this fragile QS from environmental thermal perturbations.

To investigate the influence of the magnon-Kerr nonlinearity on the noise-tolerant quantum synchronization, we plot the quantum synchronization measure $\mathcal{S}_Q$ as a function of the thermal excitations $\bar{n}_j$ and the magnon-Kerr-nonlinearity strength, as shown in Fig. S8. We reveal that in the magnon-Kerr-off regime, i.e., K = 0, quantum synchronization of the opto-mechanical and magnon-mechanical vibrations emerges only in the low-phonon-number regime; while in the magnon-Kerr-on regime, i.e., K < 0, it can persist to an extremely high thermal phonon numbers. Specifically, the influence of the thermal noise and the magnon-Kerr nonlinearity on the quantum synchronization can be studied in detail, by displaying the quantum synchronization measure $\mathcal{S}_Q$ versus the thermal phonon numbers in both the magnon-Kerr-off (i.e., K = 0) and magnon-Kerr-on (i.e., K < 0) regimes, as shown in Figs. S8(a) and S8(b). We find that in the magnon-Kerr-off case, quantum synchronization of the two phonon modes are deteriorated; whereas it revives once employing the magnon-Kerr nonlinearity. Therefore, we can confirm that a stronger magnon-Kerr nonlinearity leads to a larger noise-tolerant quantum synchronization, which is generated via the magnon-Kerr mechanism. This means that the magnon-Kerr nonlinearity provides a feasible way to create and protect fragile quantum resources against thermal noise, and build a noise-tolerant quantum device and a quantum-synchronization switch.

In particular, quantum synchronization of the opto- and magnon-mechanical vibrations can be switched on and off on demand by simply engineering the magnon-Kerr-nonlinearity effect.

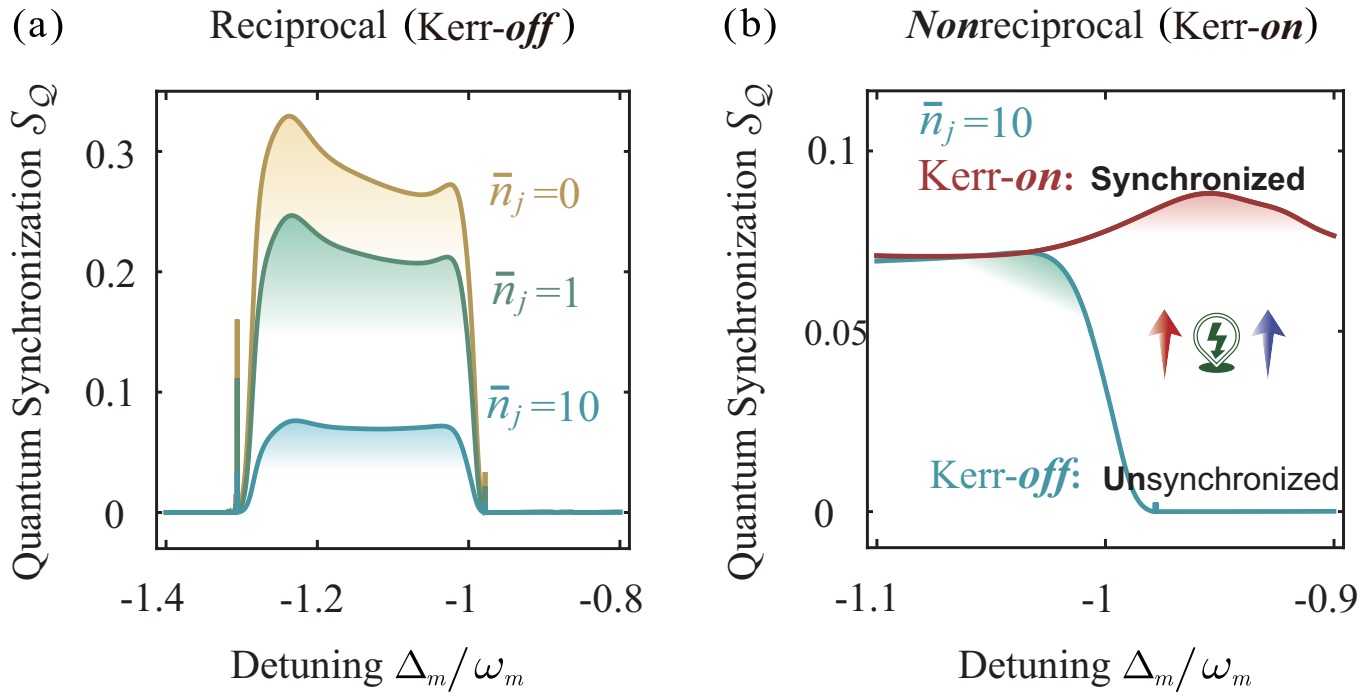

FIG. S8: Strong suppressive effect of quantum synchronization due to thermal noise, and quantum nonreciprocal revival resulted from the magnon-Kerr-induced compensation. (a) In the absence of the magnon-Kerr effect (K = 0), $\mathcal{S}_Q$ versus the magnon detuning Δ_m with the increasing thermal phonon number $\bar{n}_j$ = 0, 1, and 10. (b) For $\bar{n}_j$ = 10, $\mathcal{S}_Q$ versus Δ_m when $K/\omega_1 = -2\times10^{-5}$ and 0. For $K/\omega_1 = -2\times10^{-5}$, quantum synchronization is enhanced, reaching almost that as in an ideal device without thermal noise ($\bar{n}_j$ = 0).

(i) For example, in the high-phonon-number regime, quantum synchronization is destroyed (i.e., $\mathcal{S}_Q = 0$) because of the absence of the magnon-Kerr nonlinearity (i.e., K = 0); while by inducing the magnon-Kerr-nonlinearity effect (i.e., K < 0), quantum synchronization channel is fully turned on (i.e., $\mathcal{S}_Q > 0$). Particularly, an optimal strength of the magnon-Kerr nonlinearity (i.e., $K/\omega_1 = -2\times10^{-5}$) leads to a strong quantum synchronization.

(ii) Additionally, we find that in the high-phonon-number regime, there exists the quantum synchronization, and then the quantum synchronization is created (i.e., $\mathcal{S}_Q > 0$) in the magnon-Kerr-on regime (i.e., K < 0), while no quantum synchronization occurs (i.e., $\mathcal{S}_Q = 0$) in the magnon-Kerr-off regime (i.e., K = 0). This indicates that a selective quantum synchronization switch can be achieved just introducing a magnon-Kerr nonlinearity.

These findings underscore the potential of one-way quantum synchronization as a transformative approach to rendering noise-sensitive setups ideally suited for practical applications. This advancement holds promise for realizing noise-insensitive quantum resources, thereby advancing the frontier of quantum technologies.

Specifically, in the absence of the magnon-Kerr effect, quantum synchronization is generally deteriorated or even completely destroyed with increasing thermal occupancies; while in the presence of the magnon Kerr, it can be dramatically improved, which approaches to or even surpasses that using an ideal quantum device. This means that the noise-caused reflection can be significantly suppressed in our magnetic-Kerr device; as a result, a nearly ideal quantum synchronization can be achieved, clearly shown by defining a synchronization-revival factor:

$$\Lambda = \frac{\max[\mathcal{S}_Q(\bar{n}_j \neq 0, \mathrm{K} \neq 0)]}{\max[\mathcal{S}_Q(\bar{n}_j = 0, \mathrm{K} = 0)]}. \tag{S64}$$

We elucidate the variations in the synchronization-revival factor under the influence of thermal noise, providing insight into the dynamic interplay between environmental perturbations and synchronization phenomena. Quantum synchronization can survive in the magnon-Kerr-on regime, even when it is completely destroyed by thermal noise in the magnon-Kerr-off regime. Specifically, we demonstrate that the maximal revival factor can achieve a remarkable 99%, indicating that quantum synchronization within such a nonreciprocal device exhibits a near-robustness to thermal noise.

Remarkably, its threshold thermal phonon number for maintaining quantum synchronization is much higher than that in the case without the magnetic Kerr nonlinearity. These results indicate that applying the magnetic-Kerr effect establishes not only a giant enhancement in quantum synchronization, but also offers the possibility of preventing fragile quantum resources from the disturbances of practical thermal environment. The study opens a novel approach to develop the practical device performance by harnessing the power of nonreciprocity.

4. *Effect of mass on quantum synchronization*

Quantum synchronization of mechanical resonators in the regimes of large masses, large decays, and/or high temperatures is extremely challenging, because it requires an ultra-high optical power, which introduces extraneous excessive heating and intricate instabilities.

In recent decades, significant developments have been accomplished in the quantum synchronization of mechanical resonators in the *small-mass, low-damping, and low-noise* regimes, which have been widely reported both theoretically and experimentally, using cavity optomechanical platforms [S9–S11]. However, these proposals and experiments still inherently suffer from the large-mass, large-decay, and/or high-noise limitations, which are a major challenge for the preparation of such extremely fragile quantum synchronization. The physical origin behind these obstacles is as follows:

(i) Quantum synchronization of mechanical resonators crucially depends on the strength of driving fields. Typically, a single-excitation coupling strength scales as $g = \eta x_{\rm ZPM}$, where η quantifies the coupling strength to the resonator' position $x(t)$, and $x_{\rm ZPM}$ is the zero-point motion of a mechanical resonator in the trap, $x_{\rm ZPM} \sim \sqrt{\hbar/(2m\omega_m)}$, where ω_m is the center-of-mass mechanical oscillation frequency. For a large-mass resonator, the decrease in $x_{\rm ZPM}$ with increasing mass leads to a greatly reduced coupling strength, making quantum synchronization of mechanical resonators hard to achieve.

(ii) A large-decay and/or high-temperature mechanical resonator in the large-mass regime accelerates its intrinsic thermal motion, resulting in blocking efficient quantum synchronization of mechanical resonators.

(iii) For mechanical resonators in the regimes of a large mass and/or a high temperature, their quantum synchronization requires an ultra-high driving strength, which introduces extraneous excessive heating and intricate dynamical instabilities.

In this work, we propose how to overcome these obstacles and achieve quantum synchronization of mechanical resonators by *simply* employing the magnon-Kerr effect; and we reveal its exceptional synchronization properties otherwise unachievable in conventional devices. Unlike previous schemes, where quantum resources are generally deteriorated or even fully destroyed with increasing mass, decay, and/or noise of practical devices, our approach, surprisingly, shows that it is possible to directly *shield* inherently fragile quantum synchronization against these detrimental factors [see Figs. S2(a) and S2(b)], without the need of utilizing any high-cost low-loss materials and noise filters at the expense of system's complexity [S22, S23] or any topological structures [S24–S30].

In our analytical considerations, the masses of the two mechanical oscillators are in general different, as described by m_1 and m_2. However, for convenience, in our simulations, we consider the case where the masses of the two resonators are equal. Moreover, the masses, corresponding to the results of the other plots, are $m_1 = m_2 = 100$ ng, as given in Tab. I.

Characteristics	**Nonreciprocal Quantum Synchronization**	**Nonreciprocal Quantum Steering**
Definition	Unidirectional phase, amplitude, and frequency locking between two quantum systems	One-way quantum correlations allowing state inference via local measurements
Nonreciprocity origin	Asymmetric interaction or control (via Kerr nonlinearity, Sagnac effect)	Asymmetric violation of local hidden state (LHS) models
Observables	Dynamical quantities (e.g., phase, spectrum)	Conditional measurement outcomes and steering inequalities
Directionality	One system influences another's dynamics without feedback	One party (Alice) can steer the other (Bob), but not vice versa
Applications	One-way quantum control, nonreciprocal quantum synchronization, chiral networks	One-sided quantum cryptography, entanglement certification, quantum information tasks

TABLE III: Comparison between nonreciprocal quantum synchronization and nonreciprocal quantum steering.

5. *Difference of nonreciprocal quantum synchronization and quantum steering*

Nonreciprocal quantum synchronization and nonreciprocal quantum steering [S31] both exhibit unidirectional quantum behavior in quantum systems, but arise from fundamentally different physical mechanisms.

Nonreciprocal quantum synchronization refers to asymmetric quantum dynamical locking, such as phase or frequency entrainment, between coupled quantum oscillators. This unidirectionality stems from engineered asymmetries in the considered quantum system via the Kerr nonlinearity or rotation-induced Sagnac effect, leading to one-way quantum coherence in time-domain observables, as shown in Tab. III. The resulting unidirectional quantum coherence emerges in the time evolution of system observables and reveals asymmetric quantum synchronization, as shown in Tab. III.

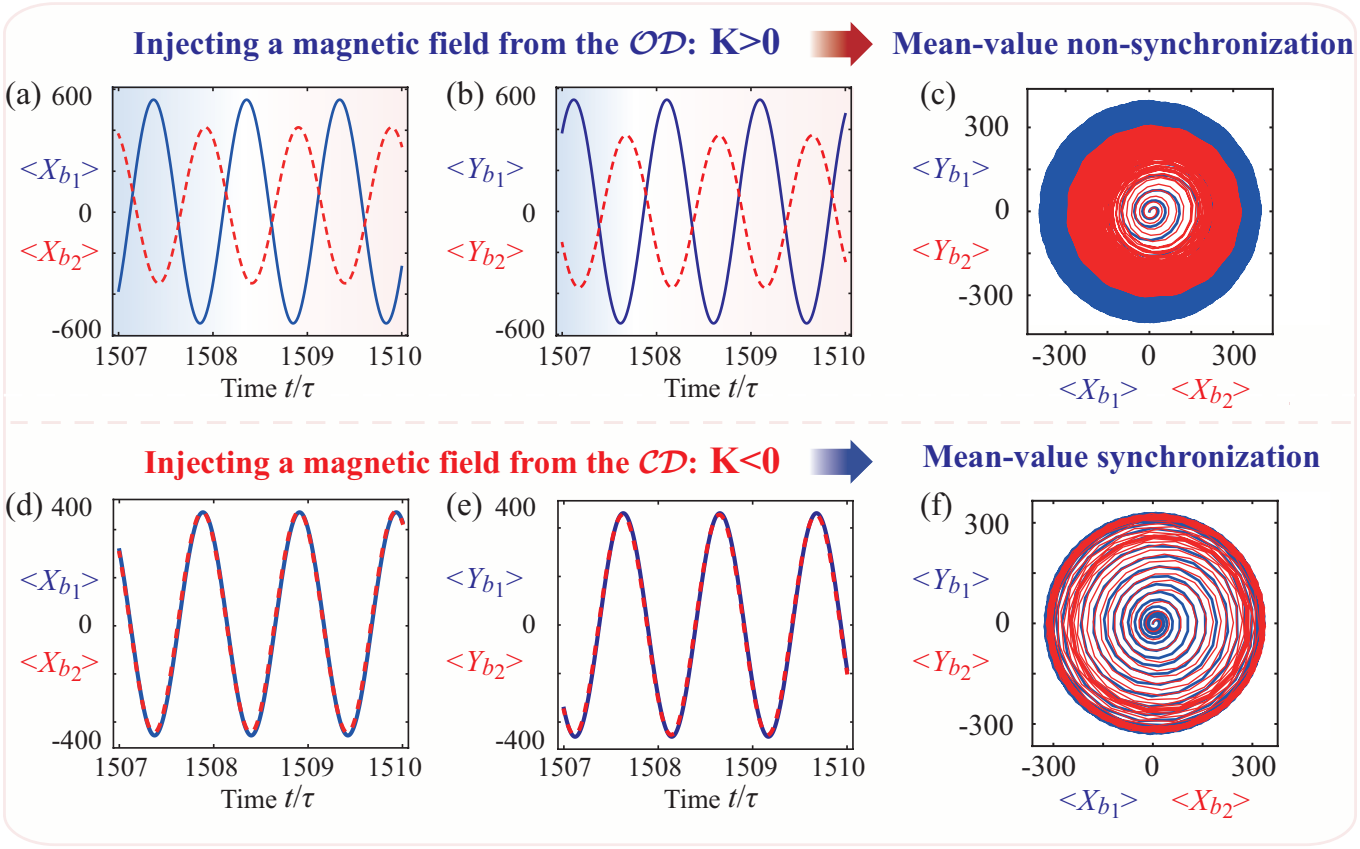

FIG. S9: Mean-value non-synchronization (in the $\mathcal{OD}$ case) and synchronization (in the $\mathcal{CD}$ case). Time evolution of (a,d) the mean values $\langle X_{b_1}(t)\rangle$ (blue solid curves) and $\langle X_{b_2}(t)\rangle$ (red dashed curves), (b,e) the mean values $\langle Y_{b_1}(t)\rangle$ (blue solid curves) and $\langle Y_{b_2}(t)\rangle$ (red dashed curves), and (c,f) the limit-cycle trajectories in the $\langle X_{b_1}(t)\rangle \rightleftharpoons \langle Y_{b_1}(t)\rangle$ and $\langle X_{b_2}(t)\rangle \rightleftharpoons \langle Y_{b_2}(t)\rangle$ spaces, when the magnetic field is applied along (a,b,c) the $\mathcal{OD}$ (i.e., K > 0) and (d,e,f) the $\mathcal{CD}$ (i.e., K < 0). Here $\Delta_m/\omega_1 = -1$ and $\Delta_a/\omega_1 = -1.005$, and other used parameters are given in Tab. I.

In stark contrast, nonreciprocal quantum steering is a form of asymmetric quantum correlation and a measurement-based manifestation of quantum nonlocality [S31], wherein one party (Alice) can nonlocally affect quantum state of another's part (Bob) through measurement, but not vice versa, as shown in Tab. III. This irreversibility reflects a directional violation of local hidden state models and underpins one-sided device-independent quantum protocols. While both phenomena break reciprocity, quantum synchronization concerns quantum dynamical behavior, whereas quantum steering reflects the structure of quantum measurement correlations. That means that unlike quantum synchronization, quantum steering does not arise from quantum dynamical evolution but from the structure of quantum measurements and conditional states, as shown in Tab. III.

B. Context of the synchronization theory

In this section, we add some discussions on our results in the context of the synchronization theory, and especially, we demonstrate that the increased resilience against both thermal fluctuations and random fabrication imperfections of the mechanical resonators arises from the magnon-Kerr nonlinearity.

First, we discuss the mean-value complete synchronization when the externally applied magnetic field is aligned parallel to either a chosen direction ($\mathcal{CD}$, i.e., [110]) or the other direction ($\mathcal{OD}$, i.e., [100]) wrt the crystallographic axes of the YIG sphere, leading to a magnon-Kerr coefficient K < 0 or K > 0, respectively. The mean-value complete synchronization requires the following conditions: $\langle X_-(t)\rangle = \langle X_{b_1}(t)\rangle - \langle X_{b_2}(t)\rangle = 0$ and $\langle Y_-(t)\rangle = \langle Y_{b_1}(t)\rangle - \langle Y_{b_2}(t)\rangle = 0$. To demonstrate this, we plot the mean values $\langle X_{b_j}(t)\rangle$ and $\langle Y_{b_j}(t)\rangle$ for $j = 1, 2$ as a function of the evolution time t, when the magnetic field enters from the $\mathcal{OD}$ and the $\mathcal{CD}$, as shown in Fig. S9. We find that though $\langle X_{b_1}(t)\rangle$ and $\langle X_{b_2}(t)\rangle$ exhibit steady oscillations, their evolutions are completely different in the $\mathcal{OD}$ case [see Fig. S9(a)]; in stark contrast to this, they become identical in the $\mathcal{CD}$ case [see Fig. S9(d)]. Meanwhile, the evolutions of $\langle Y_{b_1}(t)\rangle$ and $\langle Y_{b_2}(t)\rangle$ are completely different (same) when injecting the magnetic field from the $\mathcal{OD}$ ($\mathcal{CD}$) case, as shown in Figs. S9(b) and S9(e).

Next, we demonstrate the measure of synchronization in the context of mean-value synchronization by introducing a direct

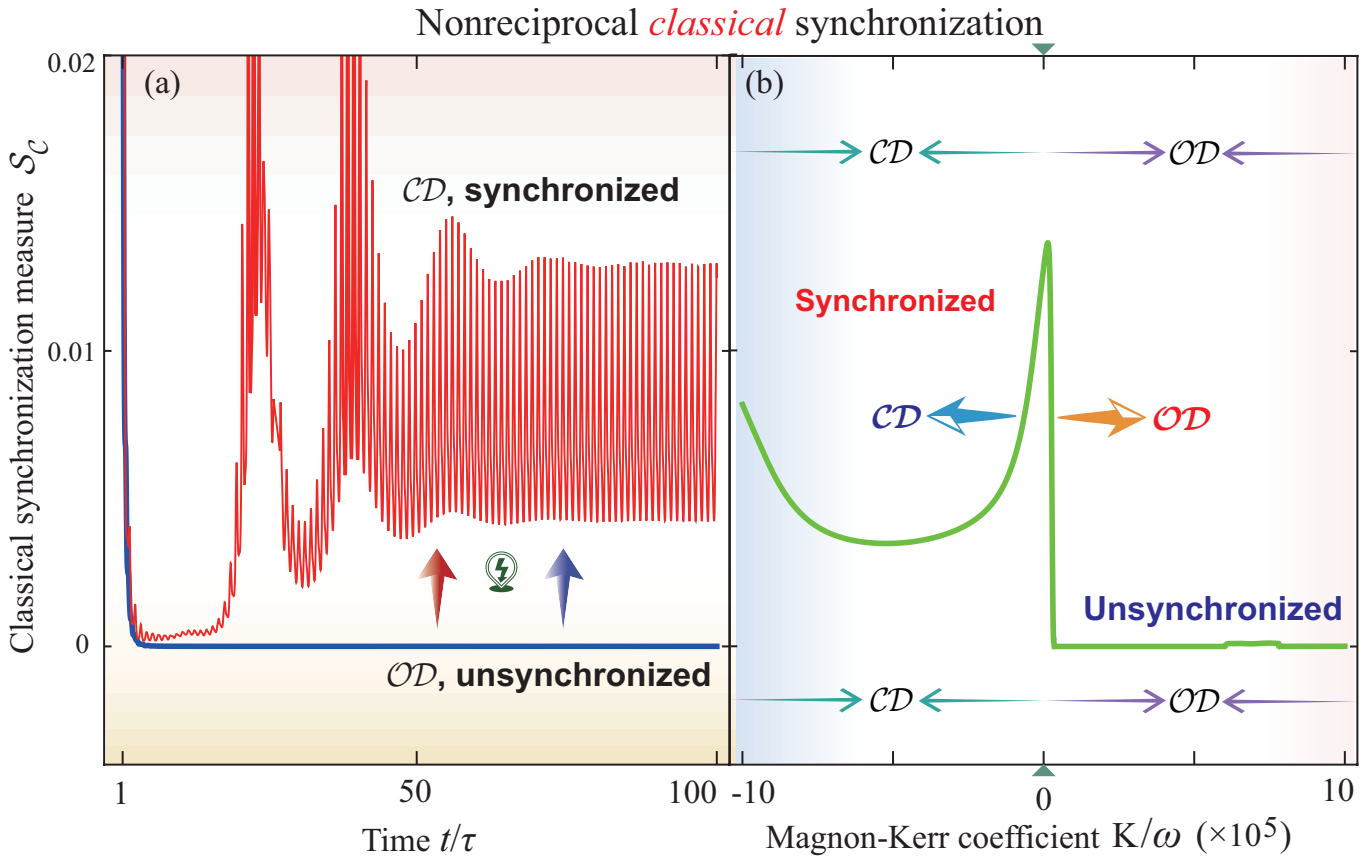

FIG. S10: (a) Classical synchronization measure $\mathcal{S}_C$ versus time t, scaled by $\tau = 2\pi/\omega_1$, when the magnetic field enters from the $\mathcal{CD}$ ($\mathrm{K}/\omega_1 = -2 \times 10^{-5}$) or $\mathcal{OD}$ ($\mathrm{K}/\omega_1 = 2 \times 10^{-5}$). (b) $\mathcal{S}_C$ versus the magnon-Kerr coefficient K. Here we set $\Omega = 0$, $\Delta_a/\omega_1 = -1.005$, and $\Delta_m/\omega_1 = -1$.

coupling between the two mechanical oscillators. The oscillation of the mean value of the position $\langle X_{b_1}(t)\rangle$ and $\langle X_{b_2}(t)\rangle$, as well as the mean values of the momentum $\langle Y_{b_1}(t)\rangle$ and $\langle Y_{b_2}(t)\rangle$, are nearly synchronized, as shown in Figs. S9(d), S9(e), and S9(f). In this scenario, the conditions for quantum synchronization are met, rendering the synchronization metrics valid. Evidently, the coupling between the two mechanical oscillators assumes a pivotal role in achieving mean-value synchronization in the nonlinear system. Furthermore, it is similar to quantum synchronization in cases where mean-value synchronization is satisfied.

In particular, beyond nonreciprocal quantum synchronization, nonreciprocal classical synchronization can also be achieved by harnessing the magnon-Kerr effect. The magnetic field aligned parallel to the $\mathcal{CD}$ of the crystallographic axes of the YIG sphere yields a redshift in the polariton frequency, whereas it applied along the $\mathcal{OD}$ leads to a blueshift. In Fig. S10(a), we show $\mathcal{S}_C(t)$ versus the time t when the magnetic field is injected from the $\mathcal{CD}$ or $\mathcal{OD}$. For the $\mathcal{CD}$ case, an efficient classical synchronization of two mechanical resonators appears ($\mathcal{S}_C \approx 0.015$, red solid curve); while for the $\mathcal{OD}$, *no* classical synchronization occurs ($\mathcal{S}_C = 0$, blue solid curve). This is because an extraordinary transition between redshift and blueshift results in the resonance and off-resonance between the magnon detuning and phonons, respectively. This demonstrates the emergence of nonreciprocal classical synchronization, that has no counterpart in the previously established demonstrations.

We also find that around $\Delta_m/\omega_1 = -1$, classical synchronization happens, because it is generated in the $\mathcal{CD}$ but vanished in the $\mathcal{OD}$, which fully agrees with the results in Fig. S10(b). Physically, the redshift (blueshift) for the $\mathcal{CD}$ ($\mathcal{OD}$) case induces a completely different physical process, where magnons are in (far-off) resonance with phonons. This indicates that, just by employing the magnon-Kerr nonlinearity, a significant classical nonreciprocity emerges. Our findings pave a route to constructing a more general nonreciprocal device beyond the limitations in classical and quantum regimes, and bridging quantum and classical nonreciprocity.

Now, we show how to achieve a significant improvement in the resilience against both thermal fluctuations and random fabrication imperfections of the resonators, just by introducing the magnon-Kerr nonlinearity. In particular, we further demonstrate that this enhanced resilience plays an important role in improving the performance of quantum synchronization. The phonon modes are thermalized by their thermal baths through the effective mechanical dissipation channels, and thermal noise can destroy fragile quantum synchronization in practical devices. Below, we study the effect of the magnon-Kerr effect

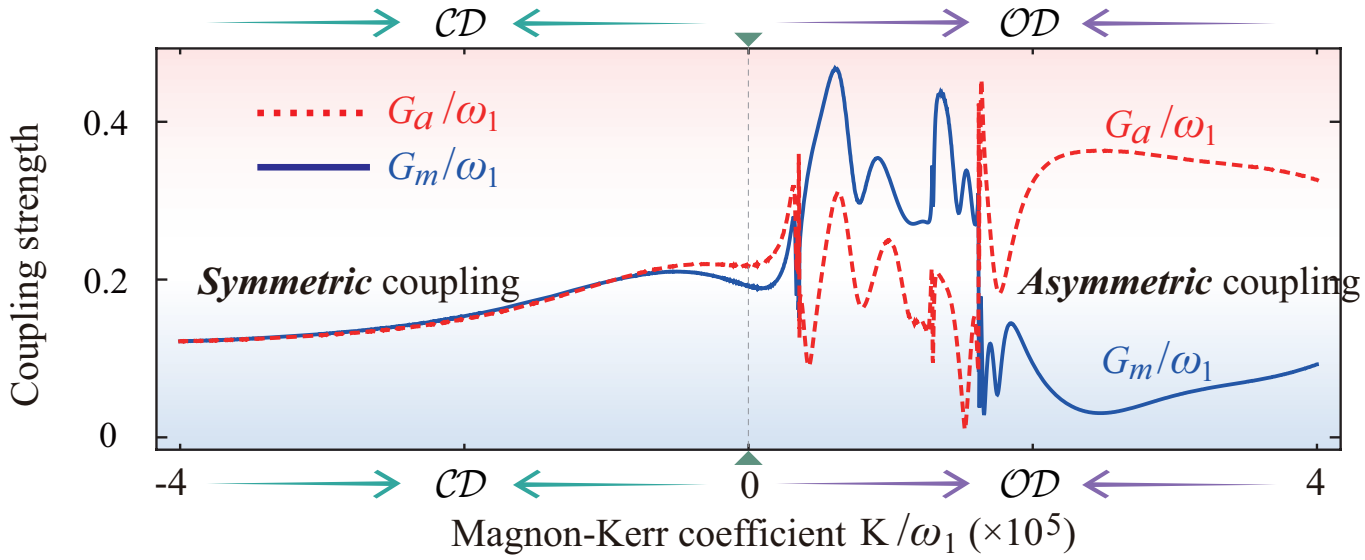

FIG. S11: Effective coupling G_m of the magnon and first phonon mode and the effective coupling G_a of the photon and second phonon mode versus the magnon-Kerr coefficient K. The magnetic field entering from the $\mathcal{CD}$ results in a symmetric coupling ($G_m \approx G_a$), corresponding to enhancing the resilience against both thermal fluctuations and random fabrication imperfections of the resonator; while the magnetic field injected from the $\mathcal{OD}$ leading to an asymmetric coupling ($G_m \neq G_a$), corresponding to reducing the resilience of the resonator. Here, the mechanical frequencies of the two mechanical modes are set as $\omega_2/\omega_1 = 1.005$, indicating the resonance of the two phonon modes.

on the effective mechanical decay rates $\Gamma_{j,\mathrm{eff}}$ when the magnon-Kerr nonlinearity is absent (K = 0) and present (K < 0). Specifically, we find that, by using the magnon-Kerr effect, the effective mechanical damping rate $\Gamma_{j,\mathrm{eff}}$ can be significantly tuned. For example, we have demonstrated that compared with the magnon-Kerr-off case, the effective mechanical dissipation rate becomes much smaller in the $\mathcal{CD}$ case, giving rise to improving the resilience of the resonator; while the effective mechanical decay rate becomes much larger in the $\mathcal{OD}$ case, resulting in reducing the resilience of the resonator. Physically, the thermal-noise-exchange rates between the mechanical resonators and their effective heat baths are much slower for a smaller value of the decay rate, and it is good for protecting quantum synchronization from environmental thermal perturbations. This significant enhancement in the resonator resilience against both thermal fluctuations and random fabrication imperfections of quantum devices plays an important role in improving the performance of quantum synchronization. These findings demonstrate that the increase in the synchronization measure for a $\mathcal{CD}$ mode applied field is a consequence of the enhanced resilience of the resonator.

To further demonstrate that the implementation of the magnon-Kerr effect enhances the resilience against both thermal fluctuations and random fabrication imperfections of the resonator, we plotted the effective magnon-phonon (G_m) and photon-phonon (G_a) coupling strengths as a function of the magnon-Kerr coefficient K in Fig. S11. We reveal that injecting the magnetic field from the $\mathcal{CD}$ yields a symmetric coupling ($G_m \approx G_a$), corresponding to an improvement in the resonator resilience; while applying it from the $\mathcal{OD}$ leads to an asymmetric coupling ($G_m \neq G_c$), corresponding to a decrease in the resilience.

C. Potential applications

While the primary focus of our work is on fundamental aspects of nonreciprocal quantum synchronization and one-way nonclassical correlations, our results have potential implications for unidirectional quantum information processing, particularly in the context of quantum entanglement distribution, quantum sensing, and the design of robust quantum networks [S18, S31–S34]. The nonreciprocal quantum-synchronization-induced correlations could serve as a key quantum resource for stabilizing quantum coherence across distributed systems, even in the presence of noise or disorder [S18, S31–S34], as shown in Tab. IV. To highlight the potential applications and advantages of our findings, we present the following discussions.

The demonstrated nonreciprocal control of quantum synchronization in this platform may find use in unidirectional quantum information processing, where synchronized quantum systems can serve as robust building blocks for distributed quantum networks [S18, S31–S34]. The tunable magnon-Kerr nonlinearity effect and its resilience to random fabrication imperfections of practical devices suggest possible applications in quantum sensing and quantum signal transduction, especially in noisy or imperfect environments. Our robustness analysis provides insights relevant for the design of scalable chiral quantum networks, where fabrication-induced imperfections are inevitable. These findings may also contribute to future developments in

nonreciprocal quantum sensing architectures that exploit collective dynamics for enhanced quantum precision [S18, S31–S34].

Application Area	Implications of Our Findings
Nonreciprocal quantum information processing	Enables unidirectional routing of quantum correlations in phononic or hybrid quantum networks, and enhances thermal robustness and quantum coherence preservation.
Nonreciprocal quantum state engineering	Provides a tunable Kerr-nonlinear mechanism to stabilize phase-locked mechanical states for preparing non-classical mechanical resources used in quantum sensing and quantum interface protocols.
Quantum transduction architectures	Facilitates noise-resilient quantum synchronization and temporal alignment across subsystems in hybrid quantum systems (e.g., microwave-to-optical converters), and improves quantum transduction efficiency.
Nonreciprocal quantum sensing	Robustness to fabrication imperfections enables practical quantum sensing platforms that operate reliably in noisy or imperfect environments.
Chiral quantum networks	Supports the design of scalable quantum networks resilient to disorder, with synchronized units functioning as robust quantum nodes.
Fundamental studies of irreversibility	Provides a testbed to explore entropy production and time-asymmetric quantum dynamics in open quantum systems, with applications in informing nonreciprocal quantum thermodynamics.

TABLE IV: Potential applications and broader advantages of nonreciprocal quantum synchronization.

In particular, our nonreciprocal quantum synchronization framework unlocks multiple exciting opportunities for application across quantum technologies. Including:

(i) Nonreciprocal quantum information processing.—The resulting nonreciprocal quantum synchronization enables a controllable unidirectional flow of quantum correlations (quantum information), which can be harnessed for unidirected quantum signal routing in phononic or hybrid quantum networks, where thermal robustness and coherence preservation are essential [S18].

(ii) Nonreciprocal quantum state engineering.—Our scheme offers a tunable, nonlinearity-engineered route to stabilize phase-locked mechanical states. This can be employed to prepare non-classical mechanical states, which is good for nonreciprocal quantum sensing or interface protocols between mechanical and optical (magnonic) degrees of freedom [S31, S32].

(iii) Quantum transduction architectures.—In hybrid quantum systems where mechanical resonators serve as intermediaries between disparate platforms (e.g., microwave-to-optical conversion), nonreciprocal quantum synchronization could enable efficient and noise-robust temporal alignment across subsystems [S33, S34].

(iv) Fundamental studies of irreversibility.—The intrinsic unidirectionality in the quantum synchronization dynamics constitutes a controlled setting for investigating microscopic origins of irreversibility and entropy production in open quantum systems, thus offering insights relevant to nonreciprocal quantum thermodynamics.

We believe these points illustrate the broader utility of our findings, for both potential quantum technologies and fundamental physics.

[S1] S. Maayani, R. Dahan, Y. Kligerman, E. Moses, A. U. Hassan, H. Jing, F. Nori, D. N. Christodoulides, and T. Carmon, Flying couplers above spinning resonators generate irreversible refraction, Nature (London) **558**, 569 (2018).

[S2] R. Huang, A. Miranowicz, J.-Q. Liao, F. Nori, and H. Jing, Nonreciprocal Photon Blockade, Phys. Rev. Lett. **121**, 153601 (2018).

[S3] A. Mari, A. Farace, N. Didier, V. Giovannetti, and R. Fazio, Measures of Quantum Synchronization in Continuous Variable Systems, Phys. Rev. Lett. **111**, 103605 (2013).

[S4] Y.-P. Wang, G.-Q. Zhang, D. Zhang, T.-F. Li, C.-M. Hu, and J. Q. You, Bistability of Cavity Magnon Polaritons, Phys. Rev. Lett. **120**, 057202 (2018).

[S5] Z. Shen, G.-T. Xu, M. Zhang, Y.-L. Zhang, Y. Wang, C.-Z. Chai, C.-L. Zou, G.-C. Guo, and C.-H. Dong, Coherent Coupling between Phonons, Magnons, and Photons, Phys. Rev. Lett. **129**, 243601 (2022).

[S6] J. Li, S.-Y. Zhu, and G. S. Agarwal, Magnon-Photon-Phonon Entanglement in Cavity Magnomechanics, Phys. Rev. Lett. **121**, 203601 (2018).

[S7] X. Zhang, C.-L. Zou, L. Jiang, and H. X. Tang, Cavity magnomechanics, Sci. Adv. **2**, e1501286 (2016).

[S8] M. F. Colombano, G. Arregui, F. Bonell, N. E. Capuj, E. Chavez-Angel, A. Pitanti, S. O. Valenzuela, C. SotomayorTorres, D. Navarro-Urrios, and M. V. Costache, Ferromagnetic Resonance Assisted Optomechanical Magnetometer, Phys. Rev. Lett. **125**, 147201 (2020).

[S9] T. J. Kippenberg and K. J. Vahala, Cavity optomechanics: Back-action at the mesoscale, Science **321**, 1172 (2008).

[S10] P. Meystre, A short walk through quantum optomechanics, Ann. Phys. (Berlin) **525**, 215 (2013).

[S11] M. Aspelmeyer, T. J. Kippenberg, and F. Marquardt, Cavity optomechanics, Rev. Mod. Phys. **86**, 1391 (2014).

[S12] X. Liu, J. Hu, Z.-F. Li, X. Li, P.-Y. Li, P.-J. Liang, Z.-Q. Zhou, C.-F. Li, and G.-C. Guo, Heralded entanglement distribution between two absorptive quantum memories, Nature (London) **594**, 41 (2021).

[S13] N. Ofek, A. Petrenko, R. Heeres, P. Reinhold, Z. Leghtas, B. Vlastakis, Y. Liu, L. Frunzio, S. Girvin, L. Jiang et al., Extending the lifetime of a quantum bit with error correction in superconducting circuits, Nature (London) **536**, 441 (2016).

[S14] M. Mirhosseini, A. Sipahigil, M. Kalaee, and O. Painter, Superconducting qubit to optical photon transduction, Nature (London) **588**, 599 (2020).

[S15] S. Klingler, V. Amin, S. Geprägs, K. Ganzhorn, H. MaierFlaig, M. Althammer, H. Huebl, R. Gross, R. D. McMichael, M. D. Stiles, S. T. B. Goennenwein, and M. Weiler, Spin-Torque Excitation of Perpendicular Standing Spin Waves in Coupled YIG/Co Heterostructures, Phys. Rev. Lett. **120**, 127201 (2018).

[S16] S. Maity, B. Pingault, G. Joe, M. Chalupnik, D. Assumpção, E. Cornell, L. Shao, and M. Lončar, Mechanical Control of a Single Nuclear Spin, Phys. Rev. X **12**, 011056 (2022).

[S17] S. L. Braunstein and P. van Loock, Rev. Mod. Phys. **77**, 513 (2005);

[S18] C. Weedbrook, S. Pirandola, R. García-Patrón, N. J. Cerf, T. C. Ralph, J. H. Shapiro, and S. Lloyd, Gaussian quantum information, Rev. Mod. Phys. **84**, 621 (2012).

[S19] Y.-F. Jiao, S.-D. Zhang, Y.-L. Zhang, A. Miranowicz, L.-M. Kuang, and H. Jing, Nonreciprocal Optomechanical Entanglement against Backscattering Losses, Phys. Rev. Lett. **125**, 143605 (2020).

[S20] E. X. DeJesus and C. Kaufman, Routh-Hurwitz criterion in the examination of eigenvalues of a system of nonlinear ordinary differential equations, Phys. Rev. A **35**, 5288 (1987).

[S21] A. Pikovsky, M. Rosenblum, and J. Kurths, *Synchronization: A Universal Concept in Nonlinear Sciences* (Cambridge University Press, New York, 2001).

[S22] A. Boltasseva, H. A. Atwater, Low-loss plasmonic metamaterials, Science **331**, 290 (2011).

[S23] S. M. Kuo, D. R. Morgan, Active noise control: A tutorial review, Proc. IEEE 87, 943 (1999).

[S24] R. El-Ganainy, K. G. Makris, M. Khajavikhan, Z. H. Musslimani, S. Rotter, and D. N. Christodoulides, Non-Hermitian physics and $\mathcal{PT}$ symmetry, Nat. Phys. **14**, 11 (2018).

[S25] K. G. Makris, R. El-Ganainy, D. N. Christodoulides, and Z. H. Musslimani, Beam dynamics in $\mathcal{PT}$ symmetric optical lattices, Phys. Rev. Lett. **100**, 103904 (2008).

[S26] J. M. P. Nair, D. Mukhopadhyay, and G. S. Agarwal, Enhanced Sensing of Weak Anharmonicities through Coherences in Dissipatively Coupled Anti-PT Symmetric Systems, Phys. Rev. Lett. **126**, 180401 (2021).

[S27] S. Mittal, V. V. Orre, and M. Hafezi, Topologically robust transport of entangled photons in a 2D photonic system, Opt. Express **24**, 15631 (2016).

[S28] M. A. Gorlach, A. N. Poddubny, Topological edge states of bound photon pairs, Phys. Rev. A **95**, 053866 (2017).

[S29] C. Chen, L. Jin, and R.-B. Liu, Sensitivity of parameter estimation near the exceptional point of a non-Hermitian system, New J. Phys. **21**, 083002 (2019).

[S30] H. Wang, S. Assawaworrarit, S. Fan, Dynamics for encircling an exceptional point in a nonlinear non-Hermitian system, Opt. Lett. **44**, 638 (2019).

[S31] R. Uola, A. C. S. Costa, H. C. Nguyen, and O. Gühne, Quantum steering, Rev. Mod. Phys. **92**, 015001 (2020).

[S32] A. I. Lvovsky and M. G. Raymer, Continuous-variable optical quantum-state tomography, Rev. Mod. Phys. **81**, 299 (2009).

[S33] K. Azuma, S. E. Economou, D. Elkouss, P. Hilaire, L. Jiang, H.-K. Lo, and I. Tzitrin, Quantum repeaters: From quantum networks to the quantum internet, Rev. Mod. Phys. **95**, 045006 (2023).

[S34] R. Horodecki, P. Horodecki, M. Horodecki, and K. Horodecki, Quantum entanglement, Rev. Mod. Phys. **81**, 865 (2009).